Kinetic Modelling of the Transport of Dust Particles in a Rarefied Atmosphere

Frédérique Charles[1,2], Stéphane Dellacherie[2], Jacques Segré[2]

[1] Centre de Mathématiques et de Leurs Applications,
ENS Cachan, CNRS, UniverSud,
61 Avenue du President Wilson, F-94230 Cachan.

[2]Commissariat à l'Énergie Atomique,
Laboratoire d'Études Thermohydrauliques des Réacteurs,
CEA, DEN, DM2S, SFME,
F-91191 Gif-sur-Yvette Cedex.

Abstract

We propose kinetic models to describe dust particles in a rarefied atmosphere in order to model the beginning of a *Loss Of Vacuum Accident* (LOVA) in the framework of safety studies in the *International Thermonuclear Experimental Reactor* (ITER). After having studied characteristic time and length scales at the beginning of a LOVA in ITER and underlined that these characteristic scales justify a kinetic approach, we firstly propose a kinetic model by supposing that the collisions between dust particles and gas molecules are inelastic and are given by a diffuse reflexion mechanism on the surface of dust particles. This collision mechanism allows us to take into account the macroscopic character of dust particles compared to gas molecules. This leads to establish new Boltzmann type kinetic operators that are non classical. Then, by noting that the mass of a dust particle is huge compared to the mass of a gas molecule, we perform an asymptotic expansion to one of the dust-molecule kinetic operators with respect to the ratio of mass between a gas molecule and a dust particle. This allows us to obtain a dust-molecule kinetic operator of Vlasov type whose any numerical discretization is less expensive than any numerical discretization of the original Boltzmann type operator. At last, we perform numerical simulations with Monte-Carlo and Particle-In-Cell (PIC) methods which validate and justify the derivation of the Vlasov operator. Moreover, examples of 3D numerical simulations of a LOVA in ITER using these kinetic models are presented.

Key words: dust particle, rarefied spray, rarefied atmosphere, kinetic operator, Boltzmann operator, Vlasov operator, asymptotic expansion.

1 Introduction

In the future *International Thermonuclear Experimental Reactor* (ITER), the abrasion of the facing surface of the tokamak by the deuterium-tritium plasma will lead to a production of a large amount of dust particles, essentially made up with the wall materials. These dust particles will lie on the inner surfaces of the tokamak after the functionning. In the case of a *Loss Of Vacuum Accident* (LOVA), the vessel filling may result in a mobilization of the dust particles, which may lead to several safety hazards, including possible release of activated dust particles or to a classical dust explosion. For these reasons, one of the aims of safety studies applied to the future ITER tokamak is to describe the evolution of dust particles in such a situation. In this context, diagnostics using optical, sampling or gravimetric systems [31, 32] are performed to study the extent of dust particle mobilization for a given set of flow conditions. At the same time, mathematical models are

investigated in order to compare numerical simulations with experimental diagnostics, and to predict the onset of dust particle mobilization.

Several models for the description of a spray constitued by solid or liquid particles in suspension in a surrounding gas are used in this framework. One can distinguish different approaches, depending on the type of the partial differential equations used to describe the gas and the (solid or liquid) particles. A first approach consists in describing the gas-particles mixture like a multiphase fluid using hydrodynamic equations, like in the Gidaspow model [29] or in the Baer & Nunziato model [2] (which is used for situation of detonation - deflagration of dusty gas). These approaches have been extended in [28] for the situation of dust particles mobilization in ITER. A major drawback of this method is that it can not deal with situations when the particles are not enough dense to be modeled as a continuous fluid.

A second approach consists in coupling an eulerian and a lagrangian approach. More precisely, the evolution of the gas is described by classical hydrodynamic equations, whereas the evolution of (solid or liquid) particles is described by a kinetic equation or by a system of ordinary differential equations. The interaction between the gas and the particles is taken into account by mean of a Stokes type drag force

$$\mathbf{F}(v,r) = \frac{D_p}{m_p(r)}\left(\mathbf{u}_g - v\right) \tag{1}$$

where D_p is an empirical coefficient depending on the surrounding gas and particles, $\mathbf{u}_g(t,x)$ is the macroscopic velocity of the gas and $m_p(r)$ is the mass of a particle of radius r. We refer to [33, 24, 25] for examples for such kinetic-fluid models in the case of thin polydispersed sprays and to [35] in the case of thick sprays (which are used for example in the code KIVA II [36]). This approach is used in the accidental situation of a LOVA in ITER in [43], [8] and [37], where it is shown by numerical simulations that dust particles may be mobilized. Moreover, Takase [43] shows also that the crucial phenomenoms take place during the beginning of the LOVA that is to say during the first milliseconds. However, the atmosphere inside the vessel is initially rarefied, and hydrodynamic models are consequently not suitable to describe the flow of the gas just after the air ingress in the vessel. Indeed, it is possible to compute some Knudsen numbers associated to this situation such as

$$\begin{cases} Kn_{21} := \dfrac{\lambda_{21}}{\delta_{dust}}, \\ \\ Kn_{22} := \dfrac{\lambda_{22}}{d} \end{cases} \tag{2}$$

where λ_{21} and λ_{22} are the mean free pathes of gas molecules respectively for the dust-molecule collisions and for the molecule-molecule collisions. In (2), $\delta_{dust} := \frac{1}{{n_1^\circ}^{1/3}}$ may be seen as an average distance between dust particles at the macroscopic level [6] – n_1° being an order of magnitude of the number density of dust particles – and d is a characteristic length scale of the emissive source that is responsible for the LOVA in ITER. Then, by supposing for the sake of simplicity that the dust particles and the gas molecules are respectively only tungsten and N_2 (nitrogen), by taking $n_1^\circ = 10^{14}$ m^{-3} (this order of magnitude will be justified in § 2.1) and $d = 10^{-2}$ m, by supposing that the initial order of magnitude of the number density in gas molecules and the initial temperature in ITER are respectively equal to $n_2^\circ = 10^{20}$ m^{-3} and to $T^\circ = 300$ K and by supposing that the radius of a dust particle is smaller than 10^{-5} m [31], we obtain $Kn_{21} \geq 1$ and $Kn_{22} \geq 1$. As a consequence, the initial atmosphere in ITER is rarefied which justifies to model the beginning of a LOVA in ITER with a kinetic approach where, in particular, the gas molecules should not be at thermodynamical equilibrium. In other words, we have to propose a kinetic model for a spray in a rarefied gas. In [26], a kinetic model for the transport of solid particles in a gas is proposed. Nevertheless, in this approach, the gas is supposed to be at thermodynamical equilibrium and is described by a maxwelian distribution. As a consequence, the density in number of solid particles is solution of a linear kinetic equation. Another approach to model dust particles in a rarefied atmosphere is proposed in [27] for the steady evaporation from a spherical condensed phase contening solid particles. In this model, the evolution of the gas molecules is described by a BGK-Boltzmann type equation and the evolution of dust particles is described by a fluid model without pressure. A similar model has been applied later in [14] in the 3D modelling of cometary flows by Monte-Carlo simulations. Let us note that it is shown in [14] that some physical phenomena which are characteristic

of a dust-molecule flow in the coma of a comet can only be obtained with a kinetic description of the gas molecules. In [45], a dust-molecule kinetic model is proposed to model the interaction between dust particles coming from an intensive volcanic plume and a rarefied atmosphere as in the case of volcanoes on Jupiter's moon Io. In this kinetic model, the dust-molecule collisions are treated with classical (elastic) multispecies Boltzmann operators for nano-sized dust particles and with a drag model of type (1) for the micron-sized dust particles – this drag model being deduced from the classical (elastic) multispecies Boltzmann operators –, and the feedback of dust particles on the gas molecules is not taken into account.

We propose in this work purely kinetic models of Boltzmann and/or Vlasov type to describe the dust-molecule mixture. These models are devoted to complete previous models, especially in the context of the beginning of a LOVA in ITER for which any fluid model cannot be valid since the atmosphere is initially rarefied. In particular, to take into account the fact that dust particles are macroscopic compared to molecules, we suppose that the dust-molecule collision mechanism is analogous to a *diffuse reflexion boundary condition* [13] and, thus, is inelastic, which implies that we have to introduce a random process in the multispecies kinematic relations of the dust-molecule collision. As a consequence, the proposed dust-molecule (inelastic) kinetic operators are not classical (elastic) multispecies Boltzmann operators. Let us note that the proposed dust-molecule kinetic model takes into account the feedback of the dust particles on the gas molecules, which is not the case in previous works except in [27, 45]. Moreover, we derive a Vlasov-Boltzmann type model by performing an asymptotic expansion of one of the dust-molecule kinetic operators with respect to the ratio of mass between a gas molecule and a dust particle. This allows us to obtain a dust-molecule kinetic operator whose any numerical discretization is less expensive than any numerical discretization of the original Boltzmann type model. Let us note that the obtained Vlasov operator allows us to generalize the dust-molecule drag model (1) to a rarefied atmosphere where the dust-molecule interaction is inelastic. At last, let us underline that the proposed dust-molecule kinetic models could also describe the interaction between dust particles coming from an intensive volcanic plume and a rarefied atmosphere as, for example, in the case of volcanoes on Jupiter's moon Io [44, 45].

The outline of this paper is the following: In Section 2, we introduce basic modelling hypothesis and we estimate characteristic time and length scales in the context of a LOVA in ITER. This allows us, firstly, to justify the fact that dust-dust collisions may not be taken into account in this context, secondly, to justify the use of a kinetic model to describe the beginning of a LOVA in ITER, and, thirdly, to justify the fact that the dust-molecule kinetic model cannot be a *classical* (elastic) multispecies Boltzmann model because of the macroscopic character of dust particles compared to gas molecules. Then, we introduce the general formulation of the proposed dust-molecule kinetic model. In Section 3, we derive the Boltzmann type operators which model the dust-molecule collisions. In Section 4, we derive a Vlasov-Boltzmann type model by performing an asymptotic expansion. In Section 5, we study the dust-molecule kinetic model of Vlasov-Boltzmann type at different time and length scales. This study allows us to estimate the appropriate characteristic time and length scales of the proposed kinetic modelling in the context of a LOVA in ITER, which is in particular important for numerical simulations. In Section 6, we propose numerical simulations with Monte-Carlo and Particle-In-Cell (PIC) methods. These numerical results validate and justify the derivation of the dust-molecule kinetic operator of Vlasov type. Moreover, examples of 3D numerical simulations of a LOVA scenario using the proposed dust-molecule kinetic models are presented. At last, we conclude in Section 7.

2 Formulation of the dust-molecule kinetic model

To propose a dust-molecule kinetic model of Boltzmann and/or Vlasov type, we have to clearly introduce modelling hypothesis and to estimate time scales, length scales and Knudsen numbers in the physical context of a LOVA in ITER. This analysis, firstly, justifies the fact that dust-dust collisions may not be taken into account in the model, secondly, justifies the use of a kinetic model to describe the beginning of a LOVA in ITER, and, thirdly, justifies the fact that the dust-molecule kinetic model cannot be a *classical* (elastic) multispecies Boltzmann model because of the macroscopic character of dust particles compared to gas molecules. In particular, we briefly discuss the impact of the magnitude of the dust particle radius on the *diluted gas hypothesis* and on the *molecular chaos hypothesis*.

2.1 Basic modelling hypothesis

We introduce basic modelling hypothesis which will be used, in particular, to justify in § 2.2.3 the fact that the beginning of a LOVA in ITER has to be modelled with a kinetic modelling.

2.1.1 Hypothesis on the physical properties of dust particles and gas molecules

The first hypothesis concerns the incompressibility and the shape of dust particles and gas molecules:

Hypothesis 1 *Dust particles and molecules are supposed to be hard spheres of respective radius r and r_2. Moreover, we suppose that*

$$r \in [r_{min}, r_{max}] \qquad with \qquad 0 < r_{min} < r_{max} < +\infty.$$

In the context of ITER, a large size distribution range is expected for dust particles, with radius included between 10^{-8} m and 10^{-5} m [41]. However, we focus here our attention on the biggest of those dust particles, and we take $r_{min} \simeq 10^{-6}$ m and $r_{max} \simeq 10^{-5}$ m.

The tricky point of our modelling is the large difference in size between dust particles and gas molecules. Thus, considering for the sake of simplicity that the gas is constituted of only one type of molecule, we make this second hypothesis:

Hypothesis 2 *Dust particules are supposed to be macroscopic compared to gas molecules which means that*

$$\frac{r_2}{r_{min}} \ll 1. \tag{3}$$

By supposing that gas molecules are nitrogen N_2 in the rarefied atmosphere, we have $r_2 \simeq 2 \cdot 10^{-10}$ m which implies that $r_2/r_{min} \simeq 2 \cdot 10^{-4}$.

A consequence of Hypothesis 2 concerns the magnitude of the mass of a dust particle compared to the magnitude of the mass of a gas molecule:

Hypothesis 3 *The mass m_2 of a molecule is very low compared to the mass $m_1(r)$ of a dust particle of radius r. In other words, we assume that*

$$\varepsilon_m \ll 1 \tag{4}$$

with

$$\begin{cases} \varepsilon_m := \varepsilon(r_{min}), & (a) \\ \varepsilon(r) := \dfrac{m_2}{m_1(r)}. & (b) \end{cases} \tag{5}$$

Of course, (4) implies that

$$\forall r \in [r_{min}, r_{max}] : \quad \varepsilon(r) \ll 1 \tag{6}$$

since $m_1(r) = \frac{4}{3}\pi\rho r^3$ where ρ is the volumic mass of the chemical component of dust particles. Hypothesis 2 and 3 *are not equivalent but are linked.* Indeed, by defining the dimensionless constant

$$\eta := \frac{3m_2}{4\pi\rho r_2^3}, \tag{7}$$

we have

$$\varepsilon(r) = \left(\frac{r_2}{r}\right)^3 \eta. \tag{8}$$

Thus, Hypothesis 2 only implies that

$$\left(\frac{\varepsilon_m}{\eta}\right)^{1/3} \ll 1. \tag{9}$$

Relation (8) shows that Hypothesis 3 is satisfied under Hypothesis 2 *when η is not too high.* In the context of ITER, by only considering dust particles of tungsten (which is the heaviest material that should be considered) and by only considering nitrogen N_2 in the rarefied atmosphere, we have $\rho = 19,3 \cdot 10^3$ kg·m^{-3}, $r_2 \simeq 2 \cdot 10^{-10}$ m and $m_2 = 4,6 \cdot 10^{-26}$ kg. Thus, we obtain $\eta \simeq 7,2 \cdot 10^{-2}$ which implies that Hypothesis 3 is satisfied.

2.1.2 Hypothesis on the initial thermodynamic state

The kinetic modelling of the dust-molecule mixture consists in introducing two density functions $f_1 := f_1(t,x,v,r)$ and $f_2 := f_2(t,x,v)$ which respectively represent the number density in dust particules and in gas molecules at the time $t \in [0,T]$, at the position $x \in \Omega \subset \mathbb{R}^3$ and at the velocity $v \in \mathbb{R}^3$. In our context, the subset Ω defines the interior of the ITER tokamak, and the LOVA is produced by a small opening on the frontier $\partial\Omega$. We make two hypothesis on these number densities f_1 and f_2 which are especially adapted at the beginning of a LOVA in ITER and which will allow us to introduce characteristic time and length scales in § 2.2.1 and 2.2.2.

The first one of these two hypothesis is the following:

Hypothesis 4 *The order of magnitude of the dust particle number density n_1 is very low compared to the order of magnitude of the gas molecule number density n_2 knowing that*

$$\begin{cases} n_1(t,x) := \displaystyle\int_{\mathbb{R}^3} \int_{r_{min}}^{r_{max}} f_1(t,x,v,r)dvdr, \\ \\ n_2(t,x) := \displaystyle\int_{\mathbb{R}^3} f_2(t,x,v)dv. \end{cases}$$

More precisely, we assume that

$$\alpha^\circ \ll 1 \tag{10}$$

where

$$\alpha^\circ := \frac{n_1^\circ}{n_2^\circ} \tag{11}$$

with the two orders of magnitude

$$\begin{cases} n_1^\circ := \displaystyle\sup_{[0,T]\times\Omega} n_1(t,x) < +\infty, \\ \\ n_2^\circ := \displaystyle\inf_{[0,T]\times\Omega} n_2(t,x) > 0. \end{cases}$$

Moreover, in the context of a LOVA in ITER, we suppose that

$$\begin{cases} \displaystyle\sup_{\Omega} n_1(t=0,x) \simeq n_1^\circ, \\ \\ \displaystyle\inf_{\Omega} n_2(t=0,x) \simeq n_2^\circ. \end{cases} \tag{12}$$

Let us underline that by defining n_1° and n_2° respectively with the supremum of $n_1(\cdot,\cdot)$ and with the infimum of $n_2(\cdot,\cdot)$ on $[0,T]\times\Omega$, under (10), we assume that the number density of dust particles is always negligible compared to the number density of molecules during a LOVA in ITER. Let us estimate n_1° in the context of ITER. We considere the situation where the abrasion of the walls leads to the formation of $M = 10^2$ kg of tungsten mobilizable dust particles (this value corresponds to the safety limit which has been set inside the vacuum vessel, and could be reached after approximately 500 plasma pulses [32]). Then, with the estimate that the total surface of vessel is $S = 5 \cdot 10^2$ m^2, this quantity of dust particles corresponds to a width $h = M/(\rho S) = 10^{-5}$ m of eroded tungsten. Moreover, we assume that at the initial time $t = 0$ (just after the beginning of the air ingress in the vacuum vessel), dust particles are hanging uniformly in a layer of $l = 10^{-2}$ m width on the surface of the vessel. Then, the density n_1 of dust particles in this layer verifies for dust particles of radius r

$$\frac{4}{3}\pi r^3 n_1 l S = Sh.$$

Thus, when $r \in [r_{min}, r_{max}]$, we have

$$\frac{3h}{4\pi r_{max}^3 l} \leq n_1 \leq \frac{3h}{4\pi r_{min}^3 l}, \tag{13}$$

that is to say

$$2,5 \cdot 10^{11}\,\mathrm{m}^{-3} \leq n_1 \leq 2,5 \cdot 10^{14}\,\mathrm{m}^{-3}. \tag{14}$$

Consequently, we can choose in our context the order of magnitude $n_1^\circ = 10^{14}$ m^{-3}. Moreover, when there will be thermonuclear reactions in ITER, the pressure and the temperature inside the ITER tokamak will be respectively of the order of 1 atm and of $1,5 \cdot 10^8$ K. As a consequence, by using the perfect gas law, we find that the number density inside the ITER tokamak has to be of the order of 10^{20} m^{-3}. As a consequence, we choose $n_2^\circ = 10^{20}$ m^{-3}. Consequently, we have $\alpha^\circ = 10^{-6}$.

The second one of these two hypothesis concerns the order of magnitude of the kinetic temperature of each species:

Hypothesis 5 *The kinetic temperatures involved in the mixture are of the same order of magnitude. Thus, we assume that*

$$\begin{cases} T_{f_1}(t,x,r) := \dfrac{m_1(r)}{3k_B n_1(t,x,r)} \left[\displaystyle\int_{\mathbb{R}^3} f_1(t,x,v,r) \left(v - \mathbf{u}_{f_1}(t,x,r)\right)^2 dv \right], & (a) \\ \\ T_{f_2}(t,x) := \dfrac{m_2}{3k_B n_2(t,x)} \left[\displaystyle\int_{\mathbb{R}^3} f_2(t,x,v) \left(v - \mathbf{u}_{f_2}(t,x)\right)^2 dv \right] & (b) \end{cases} \tag{15}$$

where

$$\begin{cases} \mathbf{u}_{f_1}(t,x,r) := \displaystyle\int_{\mathbb{R}^3} f_1(t,x,v,r) v dv \\ \\ \mathbf{u}_{f_2}(t,x) := \displaystyle\int_{\mathbb{R}^3} f_2(t,x,v) v dv \end{cases} \tag{16}$$

verify

$$\textit{and} \qquad T_{f_2} \simeq T^\circ,$$

and, as soon as particles are mobilized,

$$T_{f_1} \simeq T^\circ.$$

In (15), $k_B \simeq 1,38 \cdot 10^{-23}$ m$^2\cdot$ kg$\cdot$ s$^{-2}\cdot$ K^{-1} is the Boltzmann's constant. Hypothesis 5 means that we suppose that there is a LOVA when the temperature in ITER is not too high that is to say when ITER is stopped. In this context, we can choose $T^\circ \simeq 300$ K. Let us underline that when $n_2^\circ \simeq 10^{20}$ m^{-3} and $T^\circ \simeq 300$ K, the perfect gas law $P_2^\circ = n_2^\circ k_B T^\circ$ gives a pressure of $P_2^\circ \simeq 4 \cdot 10^{-6}$ atm, which justifies to model, when ITER is stopped, the beginning of a LOVA with a kinetic model: we detail this question in § 2.2.3.

2.1.3 A last basic modelling hypothesis

The last basic modelling hypothesis is essentially introduced for the sake of simplicity:

Hypothesis 6 *We neglect any external force field as magnetic field.*

However, although gravity field is not written in the model for a sake of simplicity, it is taken into account in the spatially inhomogeneous 3D-simulations of § 6.2.3 and § 6.2.4. In the context of a LOVA in ITER, it is obvious that Hypothesis 1-4 cannot be affected by any external force field. Nevertheless, we may think that Hypothesis 5 could be affected by the high external magnetic field since, in that case, the dust particles of tungsten are heated by the hot hydrogen plasma or directly by the magnetic field (tungsten is a metal). Of course, when ITER is stopped, this potential problem does not exist.

2.1.4 Summary of the order of magnitudes

We now summarize the order of magnitude introduced in the previous subsections:

$$\begin{cases} r_2 &= 2 \cdot 10^{-10}\,\mathrm{m}, & \text{(a)} \\ r_{min} &= 10^{-6}\,\mathrm{m}, & \text{(b)} \\ r_{max} &= 10^{-5}\,\mathrm{m}, & \text{(c)} \\ m_2 &= 4,6 \cdot 10^{-26}\,\mathrm{kg}, & \text{(d)} \\ \rho &= 19,3 \cdot 10^{3}\,\mathrm{kg \cdot m^{-3}}, & \text{(e)} \\ T^{\circ} &= 300\,\mathrm{K}, & \text{(f)} \\ \alpha^{\circ} &= 10^{-6}, & \text{(g)} \\ n_1^{\circ} &= 10^{14}\,\mathrm{m^{-3}}, & \text{(h)} \\ n_2^{\circ} &= 10^{20}\,\mathrm{m^{-3}}. & \text{(i)} \end{cases} \tag{17}$$

We recall that these orders of magnitude are characteristic of those at the beginning of a LOVA in ITER.

2.2 Characteristic time and length scales, and Knudsen numbers

Let us now make a brief analysis of the orders of magnitude of time scales, length scales and Knudsen numbers.

2.2.1 Characteristic time scales

In order to point out the various characteristic time scales involved in the system, we make a brief analysis of the orders of magnitude of the *mean collision time* of each collision type in the dust-molecule mixture. We distinguish four types of collision which, thus, define four different mean collision times t_{ij}:

- collisions between dust particles whose mean collision time is noted t_{11};
- collisions between molecules whose mean collision time is noted t_{22};
- collisions between dust particles and molecules – *from the point of view of dust particles* – whose mean collision time is noted t_{12};
- collisions between molecules and dust particles – *from the point of view of molecules* – whose mean collision time is noted t_{21}.

These four mean collision times t_{ij} define four *characteristic time scales*. Under Hypothesis 1 and 5 and *by supposing that all dust particles have the same radius* $r \in [r_{min}, r_{max}]$, the characteristic time scales t_{ij} are given by [6]

$$\begin{cases} t_{11} = \left(4\pi r^2 n_1 < V_{11}^{rel} >\right)^{-1}, & \text{(a)} \\ t_{22} = \left(4\pi r_2^2 n_2 < V_{22}^{rel} >\right)^{-1}, & \text{(b)} \\ t_{12} = \left(\pi (r + r_2)^2 n_2 < V_{12}^{rel} >\right)^{-1}, & \text{(c)} \\ t_{21} = \left(\pi (r + r_2)^2 n_1 < V_{21}^{rel} >\right)^{-1} & \text{(d)} \end{cases} \tag{18}$$

with, as soon as particles are mobilized,

$$\begin{cases} < V_{11}^{rel} >= 4\sqrt{\frac{k_B T^\circ}{\pi m_1(r)}}, \\ \\ < V_{22}^{rel} >= 4\sqrt{\frac{k_B T^\circ}{\pi m_2}}, \\ \\ < V_{12}^{rel} >=< V_{21}^{rel} >= \sqrt{\frac{8k_B T^\circ}{\pi}\left(\frac{1}{m_1(r)}+\frac{1}{m_2}\right)} \end{cases} \tag{19}$$

knowing that $< V_{ij}^{rel} >$ is the thermal relative velocity between particles of type i and particles of type j supposed to be hard spheres [6]. Then, under Hypothesis 2-4, we have

$$\begin{cases} \frac{t_{21}}{t_{11}} \simeq 4\sqrt{2\varepsilon(r)} \ll 1, & \text{(a)} \\ \\ \frac{t_{12}}{t_{22}} \simeq 4\sqrt{2}\left(\frac{r_2}{r}\right)^2 \ll 1 & \text{(b)} \\ \\ \frac{t_{12}}{t_{21}} = \frac{n_1}{n_2} \leq \alpha^\circ \ll 1. & \text{(c)} \end{cases} \tag{20}$$

Moreover, we have also under Hypothesis 2 and 3

$$\frac{t_{22}}{t_{21}} \simeq \frac{1}{4\sqrt{2}}\frac{n_1}{n_2}\left(\frac{r}{r_2}\right)^2 \tag{21}$$

and consequently

$$\forall (t,r) \in 0 \times [r_{min}, r_{max}] \quad \frac{1}{4\sqrt{2}}\alpha^\circ\left(\frac{r_{min}}{r_2}\right)^2 \leq \frac{t_{22}}{t_{21}} \leq \frac{1}{4\sqrt{2}}\alpha^\circ\left(\frac{r_{max}}{r_2}\right)^2. \tag{22}$$

In the same way, we have under Hypothesis 4

$$\forall (t,r) \in \mathbb{R}^+ \times [r_{min}, r_{max}] : \quad \frac{t_{22}}{t_{11}} = \frac{n_1}{n_2}\left(\frac{r}{r_2}\right)^2\sqrt{\varepsilon(r)} = \frac{n_1}{n_2}\sqrt{\eta\frac{r}{r_2}} \leq \alpha^\circ\sqrt{\eta\frac{r_{max}}{r_2}} \tag{23}$$

where η is defined by (7). By using (7) and (17), we obtain

$$\begin{cases} \frac{1}{4\sqrt{2}}\alpha^\circ\left(\frac{r_{min}}{r_2}\right)^2 \simeq 4,4, & \text{(a)} \\ \\ \frac{1}{4\sqrt{2}}\alpha^\circ\left(\frac{r_{max}}{r_2}\right)^2 \simeq 4,4\cdot 10^2, & \text{(b)} \\ \\ \alpha^\circ\sqrt{\eta\frac{r_{max}}{r_2}} \simeq 6\cdot 10^{-5}. & \text{(c)} \end{cases} \tag{24}$$

Thus, we deduce from (22), (23) and (24) that

$$\begin{cases} \forall (t,r) \in 0 \times [r_{min}, r_{max}] : & \frac{t_{22}}{t_{21}} \geq 1. \\ \\ \forall (t,r) \in \mathbb{R}^+ \times [r_{min}, r_{max}] : & \frac{t_{22}}{t_{11}} \ll 1. \end{cases}$$

Finally, in our context, the characteristic time scales t_{ij} are such that

$$\forall (t,r) \in 0 \times [r_{min}, r_{max}] : \quad t_{12} \ll t_{21} \leq t_{22} \ll t_{11}. \tag{25}$$

We deduce from (25) that the dust-dust mean collision time t_{11} is the largest characteristic time scale involved in the collisionsat the beginning of the LOVA. More precisely, hypothesis (17) implies that

$$\begin{cases} r = r_{min} : & < V_{11}^{rel} > \simeq 5,1 \cdot 10^{-4} \text{ m} \cdot \text{s}^{-1}, \\ r = r_{max} : & < V_{11}^{rel} > \simeq 1,6 \cdot 10^{-5} \text{ m} \cdot \text{s}^{-1}. \end{cases}$$

Then, we deduce that at the beginning of the LOVA, we have

$$0,5 \text{ s} \leq t_{11} \leq 1,5 \text{ s}.$$

On the other hand, the time scale t_{LOVA} in the context of the beginning of a LOVA in ITER is lower than 10^{-3} s [43]. Thus, we have

$$t_{LOVA} \ll t_{11}.$$

Therefore, *we can neglect dust-dust collisions in any modelling of the beginning of a LOVA in ITER*. Let us note that we have

$$< V_{22}^{rel} > \simeq 673 \text{ m} \cdot \text{s}^{-1}$$

which implies that at $t = 0$

$$t_{22} \simeq 3 \cdot 10^{-5} \text{ s} \quad \text{that is to say} \quad t_{22} \lesssim t_{LOVA}.$$

As a consequence, t_{22} seems to be a good time scale to study the beginning of a LOVA in ITER: we study in detail this question in Section 5 when $t_{22} \simeq t_{21}$ (see Hypothesis 8 and 9).

2.2.2 Characteristic length scales

The mean free path λ_{ij} of the collision of a particle of type i with a particle of type j *from the point of view of the particle of type* i is given by $\lambda_{ij} =< V_i > t_{ij}$ where $< V_i >=< V_{ii}^{rel} > /\sqrt{2}$ is the thermal velocity of the particle of type i. By using (18) and (19) (once again, we suppose that *all dust particles have the same radius* $r \in [r_{min}, r_{max}]$), we obtain

$$\begin{cases} \lambda_{11} = \dfrac{1}{4\sqrt{2}\pi r^2 n_1}, & \text{(a)} \\ \lambda_{22} = \dfrac{1}{4\sqrt{2}\pi r_2^2 n_2}, & \text{(b)} \\ \lambda_{12} = \sqrt{\dfrac{m_2}{m_1(r) + m_2}} \cdot \dfrac{1}{\pi (r + r_2)^2 n_2}, & \text{(c)} \\ \lambda_{21} = \sqrt{\dfrac{m_1(r)}{m_1(r) + m_2}} \cdot \dfrac{1}{\pi (r + r_2)^2 n_1}. & \text{(d)} \end{cases} \tag{26}$$

Then, under Hypothesis 2-4, we obtain

$$\begin{cases} \dfrac{\lambda_{21}}{\lambda_{11}} \simeq 4\sqrt{2}, & \text{(a)} \\ \dfrac{\lambda_{12}}{\lambda_{22}} \simeq 4\sqrt{2\varepsilon(r)} \cdot \left(\dfrac{r_2}{r}\right)^2 \ll 1, & \text{(b)} \\ \dfrac{\lambda_{12}}{\lambda_{21}} \simeq \sqrt{\varepsilon(r)} \cdot \dfrac{n_1}{n_2} \leq \sqrt{\varepsilon(r)}\ \alpha^\circ \ll 1, & \text{(c)} \end{cases} \tag{27}$$

which implies

$$\forall (t, r) \in \mathbb{R}^+ \times [r_{min}, r_{max}] : \quad \begin{cases} \lambda_{12} \ll \lambda_{11} \lesssim \lambda_{21}, \\ \lambda_{12} \ll \lambda_{22}. \end{cases} \tag{28}$$

Moreover, we have also under Hypothesis 2 and 3

$$\frac{\lambda_{22}}{\lambda_{21}} \simeq \frac{1}{4\sqrt{2}} \cdot \frac{n_1}{n_2} \cdot \left(\frac{r}{r_2}\right)^2 \tag{29}$$

which is exactly estimate (21). Thus, in our context, by using (24)(a,b) we have

$$\begin{cases} (t,r) = (0, r_{min}): & \lambda_{21} \lesssim \lambda_{22}, \\ \\ (t,r) = (0, r_{max}): & \lambda_{21} \ll \lambda_{22}. \end{cases}$$

Moreover, at $t = 0$ and by using (17) and (27), we have $\lambda_{22} \simeq 1,4 \cdot 10^{-2}$ m and

$$\begin{cases} 5,6 \cdot 10^{-6}\,\mathrm{m} \leq \lambda_{11} \leq 5,6 \cdot 10^{-4}\,\mathrm{m}, & \text{(a)} \\ \\ 7,6 \cdot 10^{-19}\,\mathrm{m} \leq \lambda_{12} \leq 2,4 \cdot 10^{-15}\,\mathrm{m}. & \text{(b)} \\ \\ 3,2 \cdot 10^{-5}\,\mathrm{m} \leq \lambda_{21} \leq 3,2 \cdot 10^{-3}\,\mathrm{m}. & \text{(c)} \end{cases} \tag{30}$$

Estimate (30)-(b) shows that λ_{12} is not an appropriate characteristic length scale *from a physical point of view*. At the opposite, λ_{11} and λ_{21} – which is of the same order as λ_{21} because of (27)(a) – and λ_{22} seem to be appropriate length scales from a physical point of view in our context. In Section 5, *we justify the fact that λ_{12} is not an appropriate length scale for the proposed dust-particle kinetic model*. As a consequence, we only use the characteristic length scales λ_{11}, λ_{21} and λ_{22} in the sequel of this Section 2.

2.2.3 Knudsen numbers

By defining the dust-molecule and molecule-molecule Knudsen numbers with

$$\begin{cases} Kn_{21} := \lambda_{21} \cdot n_1^{1/3}, \\ \\ Kn_{22} := \lambda_{22}/d \end{cases}$$

where $n_1^{-1/3} \simeq 2,15 \cdot 10^{-5}$ m and $d \simeq 10^{-2}$ m are macroscopic characteristic length scales respectively related to the dust particles and to the emissive source that is responsible for the LOVA in ITER [43], we deduce from (26) that at $t = 0$

$$Kn_{21} \geq 1,4 \tag{31}$$

for $r \leq r_{max}$ and

$$Kn_{22} \simeq 1,4. \tag{32}$$

Let us note that $Kn_{11} \simeq Kn_{21}/(4\sqrt{2})$ where $Kn_{11} := \lambda_{11} \cdot n_1^{1/3}$ since $\lambda_{11} \simeq \lambda_{21}/(4\sqrt{2})$ (see (27)(a)). *Estimates (31) and (32) justify the modelling of the beginning of a LOVA in ITER with dust-molecule and molecule-molecule kinetic models.*

2.3 Diluted gas hypothesis and molecular chaos hypothesis

In a binary gas mixture constituted of hard spheres, the classical multispiecies Boltzmann operators are valid when the mixture is *diluted* – which means that the dilution parameter $\eta_{ij} := \frac{4}{3}\pi r_i^3 n_j$ has to verify $\eta_{ij} \ll 1$ – and when the *molecular chaos hypothesis* is satisfied – which means that $\zeta_{ij} := \lambda_{ij}^3 n_j$ has to verify $\zeta_{ij} \gg 1$ – knowing that $(i,j) \in \{1,2\}^2$. In our context, we have the following estimates:

- *Diluted gas hypothesis:* We have

$$\forall t \in \mathbb{R}^+ : \quad \begin{cases} r = r_{min} : \ \eta_{11} \ll 1, & \text{(a)} \\ \\ r = r_{max} : \ \eta_{11} \simeq 4 \cdot 10^{-1}, & \text{(b)} \\ \\ \eta_{21} \ll 1 & \text{(c)} \end{cases} \tag{33}$$

and

$$t=0: \quad \begin{cases} r=r_{min}: \ \eta_{12} \simeq 4\cdot 10^2, & \text{(a)} \\ r=r_{max}: \ \eta_{12} \gg 1, & \text{(b)} \\ \eta_{22} \ll 1. & \text{(c)} \end{cases} \tag{34}$$

- *Molecular chaos hypothesis:* We have

$$\forall t \in \mathbb{R}^+: \quad \begin{cases} r=r_{min}: \quad \zeta_{11} \gg 1 \quad \text{and} \quad \zeta_{21} \gg 1 & \text{(a)}, \\ r=r_{max}: \quad \zeta_{11} \simeq 10^{-2} \quad \text{and} \quad \zeta_{21} \simeq 3,2 & \text{(b)} \end{cases} \tag{35}$$

and

$$t=0: \quad \zeta_{22} \gg 1 \tag{36}$$

(we do not estimate ζ_{12} since λ_{12} is not an appropriate characteristic length scale from a physical point of view: see § 2.2.2).

Estimates (33)(b), (34)(b) and (35)(b) show that the dust-molecule mixture may not be a *diluted gas* and/or may not satisfied the *molecular chaos hypothesis* at least *for dust particles whose radius is of the order of* $r_{max}=10^{-5}$ m: this is a direct consequence of the *macroscopic character of dust particles compared to molecules* (*cf.* Hypothesis 2). *As a consequence, the dust-molecule kinetic operators cannot be classical (elastic) multispecies Boltzmann operators at least for dust particles whose radius is of the order of* $r_{max}=10^{-5}$ *m: we propose to take into account this important characteristic in our modelling through Hypothesis 7 (see below) that introduces a random process in the dust-molecule binary collision.*

2.4 Kinetic modelling of dust-molecule collisions

Under Hypothesis 1-5 and in the context of the beginning of a LOVA in ITER, we can neglect the dust-dust collisions (see § 2.2.1). As a consequence, under Hypothesis 6, the dust-molecule kinetic model is given by

$$\begin{cases} \dfrac{\partial f_1}{\partial t} + v\cdot\nabla_x f_1 = R_1(f_1,f_2), & \text{(a)} \\ \dfrac{\partial f_2}{\partial t} + v\cdot\nabla_x f_2 = R_2(f_1,f_2) + Q(f_2,f_2), & \text{(b)} \\ (t,x,v,r) \in \mathbb{R}^+\times\Omega\times\mathbb{R}^3\times[r_{min},r_{max}] & \text{(c)} \end{cases} \tag{37}$$

where Ω is an open subset of $\mathbb{R}^3$ (which defines the interior of the ITER tokamak) and where $0<r_{min}<r_{max}$. The kinetic operator $Q(f_2,f_2)$ models collisions between gas molecules and is a classical Boltzmann operator. As these collisions are not the important point of our modelling, we consider a hard sphere model. Then, $Q(f_2,f_2)$ is given by

$$Q(f_2,f_2)(t,x,v) = \int_{\S^2}\int_{\mathbb{R}^3} \left[f_2(t,x,v')f_2(t,x,v'_\star) - f_2(t,x,v)f_2(t,x,v_\star)\right] {r_2}^2 |v-v^\star| d\sigma dv_\star \tag{38}$$

with

$$\begin{cases} v' = \dfrac{v+v_*}{2} - \dfrac{|v-v_*|}{2}\sigma, \\ v'_* = \dfrac{v+v_*}{2} + \dfrac{|v-v_*|}{2}\sigma \end{cases} \tag{39}$$

and $\sigma \in \mathbb{S}^2$. The main point of our modelling is the derivation of the kinetic operators $R_1(f_1,f_2)$ and $R_2(f_1,f_2)$ which model collisions between dust particles and gas molecules under Hypothesis 1 and 2, and which *cannot be classical (elastic) multispecies Boltzmann operators* at least when the radius of a dust particle is of the order of $r_{max}=10^{-5}$ m (see § 2.3).

2.5 Discussion about the basic modelling hypothesis

We make the following coments to summarize the physical justification of kinetic model (37) in our context:

- Hypothesis 1-5 are used in § 2.2 to estimate in our context the characteristic time and length scales and the Knudsen numbers involved in the dust-molecule mixture. In particular, we show that we have to model the beginning of a LOVA in ITER with a kinetic model and that we can neglect dust-dust collisions. In other words, under Hypothesis 6, the beginning of a LOVA has to be modelled with a kinetic model whose general formulation is given by (37).
- Hypothesis 2 is central to justify the derivation in Section 3 of the dust-molecule operators $R_1(f_1, f_2)$ and $R_2(f_1, f_2)$ in a *non-classical* way (see also § 2.3).
- Hypothesis 3 is central to perform in Section 4 an asymptotic analysis to approach $R_1(f_1, f_2)$ with a Vlasov type operator and, then, to simplify kinetic model (37) in Section 5.
- Hypothesis 6 allows us to neglect any external force field in (37). Of course, it would be simple to add *a posteriori* any external force field in (37) (as soon as Hypothesis 5 remains valid when Hypothesis 6 is not satisfied).

3 Derivation of dust-molecule kinetic operators of Boltzmann type

We now propose to derive the dust-molecule operators $R_1(f_1, f_2)$ and $R_2(f_1, f_2)$ used in the kinetic model (37) in the spirit of the derivation of the classical Boltzmann operator (38) [7]. The new point is the way we take into account in our modelling Hypothesis 1 and 2.

3.1 Random kinematic relations for the dust-molecule collision

Dust particles and gas molecules are supposed to be *hard spheres*: see Hypothesis 1. Moreover, dust particles are also supposed to be *macroscopic* compared to molecules: see Hypothesis 2. From a physical point of view, we have to take into account this important modelling hypothesis, which means in particular that kinetic operators $R_1(f_1, f_2)$ and $R_2(f_1, f_2)$ cannot be the multispecies versions of classical Boltzmann operator (38) (see section 2.3). In the case of the classical multispecies Boltzmann operator, kinematic relations (39) are given by [6]

$$\begin{cases} v_1 = v_B - \dfrac{\varepsilon(r)}{1+\varepsilon(r)}|v_2^\circ - v_1^\circ|\sigma, & \text{(a)} \\ \\ v_2 = v_B + \dfrac{1}{1+\varepsilon(r)}|v_2^\circ - v_1^\circ|\sigma & \text{(b)} \end{cases} \tag{40}$$

with $\sigma \in \S^2$ where $\varepsilon(r)$ is the ratio of masses defined by (5)(b) and where

$$v_B := \frac{1}{1+\varepsilon(r)} v_1^\circ + \frac{\varepsilon(r)}{1+\varepsilon(r)} v_2^\circ \tag{41}$$

is the barycentric velocity of the dust-molecule binary system. In (40), v_1° and v_2° are the pre-collisional velocities, v_1 and v_2 are the post-collisional velocities. In our modelling, we take into account Hypothesis 1 and 2 in the derivation of $R_1(f_1, f_2)$ and $R_2(f_1, f_2)$ by supposing that a molecule arriving on a dust particle thermalizes with molecules constituting the surface of the dust particle *within a negligible time with respect to the other characteristic time scales*, and leaves the dust particle following a half maxwellian at its surface temperature T_{surf}. In other words, we take into account Hypothesis 1 and 2 by supposing that the dust-molecule collision mechanism is analogous to a *diffuse reflexion boundary condition* (see [13] p. 104) and, thus, by introducing a random process in the multispecies kinematic relations (40):

Hypothesis 7 *The kinematic relations of the dust-molecule binary collision – which transform the pre-collisional velocities v_1° and v_2° into the post-collisional velocities v_1 and v_2 – are given by*

$$\begin{cases} v_1 = v_B - \dfrac{\varepsilon(r)}{1+\varepsilon(r)} v_r, & (a) \\ \\ v_2 = v_B + \dfrac{1}{1+\varepsilon(r)} v_r & (b) \end{cases} \tag{42}$$

where

$$v_r := v_2 - v_1 \tag{43}$$

is the post-relative velocity whose probability density h_n is given by

$$h_n(s) = \frac{1}{2\pi} \left(\frac{m_2}{k_B T_{surf}} \right)^2 (n \cdot s) \exp\left(-\frac{m_2 |s|^2}{2 k_B T_{surf}} \right) 1_{\{n \cdot s \geq 0\}}, \tag{44}$$

n being the normal vector at the tangent plan of the dust particle, oriented to the exterior of the dust particle, and $T_{surf} \in \mathbb{R}_*^+$ being the surface temperature of dust particles.

We roughly represent in Figure 1 the collision between a dust particle and a molecule. In this figure, $n = \frac{\overrightarrow{C_1 C_2}}{|\overrightarrow{C_1 C_2}|}$ where C_1 and C_2 are respectively the centers of the dust particule and of the molecule. In (44),

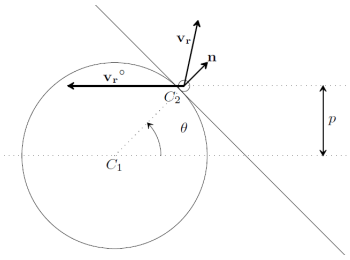

Figure 1: *Diffuse reflexion of a molecule on a dust particle*

the surface temperature of dust particles T_{surf} is not necessarily equal to the kinetic temperature T_{f_1} defined with (15)(a). For the sake of simplicity, we assume in the sequel that all dust particles have the same surface temperature T_{surf} and that T_{surf} does not depend on the time. Let us note that we can rewrite (44) with

$$h_n(s) = \frac{2\beta^4}{\pi} (n \cdot s) \exp\left(-\beta^2 |s|^2 \right) 1_{\{n \cdot s \geq 0\}} \tag{45}$$

where

$$\beta := \sqrt{\frac{m_2}{2 k_B T_{surf}}} \tag{46}$$

($1/\beta$ is a thermal velocity related to the surface temperature T_{surf} of dust particles). Of course, we can verify that

$$\forall n \in \mathbb{S}^2 : \quad \int_{\mathbb{R}^3} h_n(s) ds = 1. \tag{47}$$

Let us underline that kinematic relations (42) are such that the momentum of the dust-molecule binary system is conserved. Nevertheless, since $|v_r|$ is not equal to the pre-relative velocity $|v_r^\circ|$ with $v_r^\circ := v_2^\circ - v_1^\circ$ (see Figure 1) because of the random process, collision mechanism (42) is not planar and is not micro-reversible, and the kinetic energy is not conserved, which is not the case for the classical collision mechanism (40). This implies that the kinetic operators $R_1(f_1, f_2)$ and $R_2(f_1, f_2)$ proposed in the sequel will not verify all the properties verified by a classical (elastic) multispecies Boltzmann operator based on kinematic relations (40).

3.2 Derivation of dust-molecule operator $R_1(f_1, f_2)$

Under Hypothesis 7, $R_1(f_1, f_2)$ cannot be a classical (elastic) multispecies Boltzmann operator. To derive $R_1(f_1, f_2)$, we have to apply the heuristic Boltzmann's construction [7, 13] in the particular context of Hypothesis 7. This leads to the following proposition:

Proposition 1 *Under Hypothesis 7, the dust-molecule operator $R_1(f_1, f_2)$ obtained with the heuristic Boltzmann's construction is given by*

$$\begin{aligned} R_1(f_1, f_2)(t, x, v_1, r) =& (r + r_2)^2 \int_{\mathbb{R}^3} \int_{\mathbb{R}^3} f_1(t, x, v_1^\circ, r) f_2(t, x, v_2^\circ) B_p(v_1^\circ, v_2^\circ, v_1) dv_1^\circ dv_2^\circ \\ & - \pi (r + r_2)^2 \int_{\mathbb{R}^3} f_1(t, x, v_1, r) f_2(t, x, v_2) |v_1 - v_2| dv_2 \end{aligned} \tag{48}$$

with

$$\begin{aligned} B_p(v_1^\circ, v_2^\circ, v_1) = & \frac{2}{\pi} \beta^4 \left(\frac{1 + \varepsilon(r)}{\varepsilon(r)} \right)^4 \exp \left[-\beta^2 \left(\frac{1 + \varepsilon(r)}{\varepsilon(r)} \right)^2 (v_B - v_1)^2 \right] \\ & \times \int_{\mathbb{S}^2} [n \cdot (v_B - v_1)][n \cdot (v_1^\circ - v_2^\circ)] 1_{\{n \cdot (v_B - v_1) \geq 0\}} 1_{\left\{n \cdot (v_1^\circ - v_2^\circ) \geq 0\right\}} dn \end{aligned} \tag{49}$$

where $\varepsilon(r)$ is the ratio of masses defined by (5)(b), where v_B is the barycentric velocity given by (41) and where $1/\beta$ is a thermal velocity given by (46).

Proof of Proposition 1. In the elementary volume $dxdv_1$, the variation of the number of dust particles during the time dt is

$$\frac{df_1}{dt} dt dx dv_1 = \left(\frac{\partial f_1}{\partial t} + v_1 \cdot \nabla_x f_1 \right) dt dx dv_1.$$

Let us introduce the number of dust particles $R_1^+(f_1, f_2) dt dx dv_1$ whose position and velocity enter respectively into the classes $\lfloor x,\, x + dx \rfloor$ and $\lfloor v_1,\, v_1 + dv_1 \rfloor$, and let us also introduce the number of particles $R_1^-(f_1, f_2) dt dx dv_1$ whose position and velocity leave those classes. Then, the collisional balance writes

$$\frac{df_1}{dt} dt dx dv_1 = \left[R_1^+(f_1, f_2) - R_1^-(f_1, f_2) \right] dt dx dv_1. \tag{50}$$

Thus, the operator $R_1(f_1, f_2)$ can be expressed by

$$R_1(f_1, f_2) = R_1^+(f_1, f_2) - R_1^-(f_1, f_2). \tag{51}$$

Due to Hypothesis 1, the loss part $R_1^-(f_1, f_2)$ is a classical multispiecies Boltzmann loss operator for a hard sphere cross-section. Its expression is given by (see [13] or [11] for details)

$$R_1^-(f_1, f_2)(t, x, v_1, r) = \int_{\mathbb{R}^3} f_1(t, x, v_1, r) f_2(t, x, v_2) \pi (r + r_2)^2 |v_1 - v_2| dv_2. \tag{52}$$

We now establish the expression of $R_1^+(f_1, f_2)$ by noting that $R_1^+(f_1, f_2) dt\, dx\, dv_1$ is the number of collisions in the elementary volum dx during the time dt whose post-collisional velocity of dust particles is in the class $\lfloor v_1,\, v_1 + dv_1 \rfloor$. This number can be expressed by

$$R_1^+(f_1, f_2) dt dx dv_1 = \int_{n \in \mathbb{S}^2} \int_{v_2^\circ \in \mathbb{R}^3} \int_{v_1^\circ \in \mathbb{R}^3} l_1(v_1) dN_1^0 dv_1 \tag{53}$$

where dN_1^0 is the elementary number of collisions during the time dt in the elementary volum dx between dust particles and molecules whose pre-collisional velocities are respectively in the classes $\lfloor v_1^\circ,\, v_1^\circ + dv_1^\circ \rfloor$ and $\lfloor v_2^\circ,\, v_2^\circ + dv_2^\circ \rfloor$, and where $l_1(v_1) dv_1$ is the elementary probability that, after such a collision, the post-collisional velocity of these dust particles is in the class $\lfloor v_1,\, v_1 + dv_1 \rfloor$. At time t and at position x, the dust particles flux whose velocity is in the class $\lfloor v_1^\circ,\, v_1^\circ + dv_1^\circ \rfloor$ and relative to a molecule whose velocity is equal

to v_2° is given by $f_1(t,x,v_1^\circ)|v_1^\circ - v_2^\circ| dv_1^\circ$. Thus, the number of these dust particles that collide this molecule during a time dt with an impact parameter p and an azimuthal angle $\epsilon \in [0, 2\pi]$ (angle between a reference plan and the pre-collision plan) is equal to

$$f_1(t,x,v_1^\circ,r)|v_1^\circ - v_2^\circ|\, pdp\, d\epsilon dv_1^\circ\, dt.$$

Then, dN_1° is given by

$$dN_1^\circ = f_1(t,x,v_1^\circ,r) f_2(t,x,v_2^\circ)|v_1^\circ - v_2^\circ|\, pdpd\epsilon\, dv_1^\circ\, dv_2^\circ\, dt\, dx$$

since the number of molecules in the elementary volume dx whose velocity is in the class $\lfloor v_2^\circ,\, v_2^\circ + dv_2^\circ \rfloor$ is equal to $f_2(t,x,v_2^\circ)dv_2^\circ\, dx$. Under the assumption that dust particles and molecules are hard spheres, the impact parameter p between molecules and dust particles is given by $p = (r+r_2)\sin(\theta)$ with $\theta \in [0, \pi/2]$. Moreover, denoting n the vector $n = \frac{\overrightarrow{C_1C_2}}{|\overrightarrow{C_1C_2}|}$, where C_1 and C_2 are respectively the centers of the particule and of the molecule (see figure 1), we have

$$\begin{aligned} |v_1^\circ - v_2^\circ| pdpd\epsilon &= |v_1^\circ - v_2^\circ|(r+r_2)^2 \sin\theta\cos\theta d\theta d\epsilon \\ &= (r+r_2)^2\, [n\cdot(v_1^\circ - v_2^\circ)]\, dn \end{aligned}$$

with $n \in \mathbb{S}^2 \cap \{n\cdot(v_1^\circ - v_2^\circ) \geq 0\}$. Then, we can express dN_1° by

$$dN_1^\circ = f_1(t,x,v_1^\circ,r) f_2(t,x,v_2^\circ)\,(r+r_2)^2\,[n\cdot(v_1^\circ - v_2^\circ)]\, 1_{\left\{n\cdot\left(v_1^\circ - v_2^\circ\right)\geq 0\right\}} dn dv_1^\circ dv_2^\circ dt dx.$$

Moreover, we can express the density of probability l_1 according to the density of probability h_n of the post-collisional relative velocity $v_r := v_2 - v_1$, h_n being defined with (45). Indeed, by using (42)(a) – which implies in particular that v_B given by (41) is not changed by the collision –, we have

$$l_1(s) = \left(\frac{1+\varepsilon(r)}{\varepsilon(r)}\right)^3 h_n\left[-\frac{1+\varepsilon(r)}{\varepsilon(r)}(s - v_B)\right].$$

And, by using (45), we finally get

$$R_1^+(f_1,f_2) = \int_{\mathbb{R}^3}\int_{\mathbb{R}^3} f_1(t,x,v_1^\circ,r) f_2(t,x,v_2^\circ)(r+r_2)^2 B_p(v_1^\circ, v_2^\circ, v_1) dv_1^\circ dv_2^\circ \tag{54}$$

where $B_p(v_1^\circ, v_2^\circ, v_1)$ is given by (49). $\diamondsuit$

3.3 Derivation of dust-molecule operator $R_2(f_1,f_2)$

Following the same approach as in section 3.2, we obtain for the operator $R_2(f_1,f_2)$:

Proposition 2 *Under Hypothesis 7, the dust-molecule operator $R_2(f_1,f_2)$ obtained with the heuristic Boltzmann's construction is given by*

$$\begin{aligned} R_2(f_1,f_2)(t,x,v_2) = &\int_{r_{min}}^{r_{max}}\int_{\mathbb{R}^3}\int_{\mathbb{R}^3} (r+r_2)^2 f_1(t,x,v_1^\circ,r) f_2(t,x,v_2^\circ) B_m(v_1^\circ, v_2^\circ, v_2) dr dv_1^\circ dv_2^\circ \\ &- \int_{r_{min}}^{r_{max}}\int_{\mathbb{R}^3} \pi\,(r+r_2)^2 f_1(t,x,v_1,r) f_2(t,x,v_2)|v_2 - v_1| dr dv_1 \end{aligned} \tag{55}$$

with

$$\begin{aligned} B_m(v_1^\circ, v_2^\circ, v_2) = &\frac{2}{\pi}\beta^4 (1+\varepsilon(r))^4 \exp\left[-\beta^2(1+\varepsilon(r))^2 (v_B - v_2)^2\right] \\ &\times \int_{\mathbb{S}^2} [n\cdot(v_B - v_2)]\,[n\cdot(v_2^\circ - v_1^\circ)]\, 1_{\{n\cdot(v_B - v_2)\geq 0\}} 1_{\left\{n\cdot(v_2^\circ - v_1^\circ)\geq 0\right\}} dn \end{aligned} \tag{56}$$

where $\varepsilon(r)$, v_B and β are respectively given by (5)(b), (41) and (46).

Proof of Proposition 2. To obtain operator (55)(56), we just have to permute the subscripts 1 and 2 in operator (48)(49) (which means in particular that we replace $\varepsilon(r)$ by $1/\varepsilon(r)$) and to take into account an integration in r.$\diamondsuit$

3.4 Other formulations of dust-molecule operators $R_1(f_1, f_2)$ and $R_2(f_1, f_2)$

We now propose other formulations of the operators $R_1(f_1, f_2)$ and $R_2(f_1, f_2)$ respectively given by (48) and (55). The first ones are weak formulations of (48) and (55) ; the second ones are deduced from these weak formulations, and will be adapted for the derivation of the Vlasov-Boltzmann model in section 4. In this section, we omit the variables t and x for the sake of simplicity.

3.4.1 Weak formulation of $R_1(f_1, f_2)$ and $R_2(f_1, f_2)$

The weak formulations of $R_1(f_1, f_2)$ and $R_2(f_1, f_2)$ are given in the following proposition:

Proposition 3 *Let φ be a test function ($\varphi \in \mathcal{C}^0_c(\mathbb{R}^3)$ for example), let $R_1(f_1, f_2)$ and $R_2(f_1, f_2)$ be the Boltzmann operators* (48) *and* (55)*. Then, we have formally*

$$\int_{\mathbb{R}^3} \varphi(v) R_1(f_1, f_2)(v, r) dv = (r + r_2)^2 \int_{\mathbb{S}^2} \int_{\mathbb{R}^3} \int_{\mathbb{R}^3} \int_{\mathbb{R}^3} \left[\varphi(v_1') - \varphi(v_1)\right] f_1(v_1, r) f_2(v_2) \times h_n(w) \left[n \cdot (v_1 - v_2)\right] 1_{\{n\cdot(v_1-v_2)\geq 0\}} dn dw dv_1 dv_2 \tag{57}$$

with

$$v_1' = \frac{1}{1 + \varepsilon(r)} \left[v_1 + \varepsilon(r) v_2 - \varepsilon(r) w\right], \tag{58}$$

and

$$\int_{\mathbb{R}^3} \varphi(v) R_2(f_1, f_2)(v) dv = \int_{r_{min}}^{r_{max}} \int_{\mathbb{S}^2} \int_{\mathbb{R}^3} \int_{\mathbb{R}^3} \int_{\mathbb{R}^3} (r + r_2)^2 \left[\varphi(v_2') - \varphi(v_2)\right] f_1(v_1, r) f_2(v_2) \times h_n(w) \left[n \cdot (v_1 - v_2)\right] 1_{\{n\cdot(v_1-v_2)\geq 0\}} dr dn dw dv_1 dv_2 \tag{59}$$

with

$$v_2' = \frac{1}{1 + \varepsilon(r)} \left[v_1 + \varepsilon(r) v_2 + w\right] \tag{60}$$

where h_n is given by (44)*.*

Let us underline that under Hypothesis 3, the velocities v_1 and v_1' of a dust particle before and after a collision with a molecule are such that

$$v_1' - v_1 = \mathcal{O}(\varepsilon(r)) \tag{61}$$

(see (58)). In other words, since the mass of a dust particle is huge compared to the mass of a molecule (see Hypothesis 3), the velocity of a dust particle is few modified after a collision with a molecule. As a consequence, the collisions of dust particles on molecules are *grazing collisions*. This will allow us to approximate in section 4 the Boltzmann type operator $R_1(f_1, f_2)$ with a Vlasov type operator. Of course, the collisions of gas molecules on dust particles are not grazing collisions since

$$v_2' - v_1' = w \tag{62}$$

is not a $\mathcal{O}(\varepsilon(r))$ term (see (58) and (60)). Thus, this will not be possible to approximate the Boltzmann type operator $R_2(f_1, f_2)$ with a Vlasov type operator.

Proof of Proposition 3. Let φ be a test function and let $R_1^+(f_1,f_2)$ be the gain term (54) of the operator $R_1(f_1,f_2)$. We have

$$\int_{\mathbb{R}^3}\varphi(v)R_1^+(f_1,f_2)(v,r)dv=(r+r_2)^2\int_{\mathbb{R}^3}\int_{\mathbb{R}^3}\int_{\mathbb{R}^3}\varphi(v_1)f_1(v_1^\circ,r)f_2(v_2^\circ)B_p(v_1^\circ,v_2^\circ,v_1)dv_1^\circ dv_2^\circ dv_1 \tag{63}$$

where B_p is expressed according to h_n by

$$B_p(v_1^\circ,v_2^\circ,v_1)=\left(\frac{1+\varepsilon(r)}{\varepsilon(r)}\right)^3\int_{\mathbb{S}^2}h_n\left((v_B-v_1)\left(\frac{1+\varepsilon(r)}{\varepsilon(r)}\right)\right)\left[n\cdot(v_1^\circ-v_2^\circ)\right]1_{\left\{n\cdot(v_1^\circ-v_2^\circ)\geq 0\right\}}dn. \tag{64}$$

We set

$$w:=(v_B-v_1)\left(\frac{1+\varepsilon(r)}{\varepsilon(r)}\right)=\left(\frac{\varepsilon(r)}{1+\varepsilon(r)}v_2^\circ+\frac{1}{1+\varepsilon(r)}v_1^\circ-v_1\right)\left(\frac{1+\varepsilon(r)}{\varepsilon(r)}\right),$$

and we consider in the integral (63) the following change of variable

$$(v_1,v_1^\circ,v_2^\circ)\to(w,v_1^\circ,v_2^\circ)$$

for which the jacobian is given by

$$|J|=\left(\frac{1+\varepsilon(r)}{\varepsilon(r)}\right)^3.$$

Therefore, we get

$$\begin{aligned}\int_{\mathbb{R}^3}\varphi(v)R_1^+(f_1,f_2)(v,r)dv=&(r+r_2)^2\int_{\mathbb{S}^2}\int_{\mathbb{R}^3}\int_{\mathbb{R}^3}\int_{\mathbb{R}^3}\varphi(v_1')f_1(v_1,r)f_2(v_2)\\&\times h_n(w)\left[n\cdot(v_1-v_2)\right]1_{\{n\cdot(v_1-v_2)\geq 0\}}dndwdv_1dv_2\end{aligned} \tag{65}$$

with v_1' given by (58). Moreover, thanks to (47) and by noting that [11]

$$\forall k\in\mathbb{R}^3:\quad\int_{\mathbb{S}^2}(n\cdot k)\,1_{\{n\cdot k\geq 0\}}dn=\pi|k|, \tag{66}$$

we get the weak formulation

$$\begin{aligned}\int_{\mathbb{R}^3}\varphi(v)R_1^-(f_1,f_2)(v,r)dv=&(r+r_2)^2\int_{\mathbb{R}^3}\int_{\mathbb{R}^3}\varphi(v_1)f_1(v_1,r)f_2(v_2)\pi|v_1-v_2|dv_1dv_2\\=&(r+r_2)^2\int_{\mathbb{S}^2}\int_{\mathbb{R}^3}\int_{\mathbb{R}^3}\int_{\mathbb{R}^3}\varphi(v_1)f_1(v_1,r)f_2(v_2)\\&\times h_n(w)\left[n\cdot(v_1-v_2)\right]1_{\{n\cdot(v_1-v_2)\geq 0\}}dndwdv_1dv_2.\end{aligned} \tag{67}$$

for the loss term $R_1^-(f_1,f_2)$. Expression (57) is a direct consequence of (65) and (67). We obtain expression (59) with similar computations (see [11] for details).$\diamondsuit$

3.4.2 A second formulation of $R_1(f_1,f_2)$ and $R_2(f_1,f_2)$

We deduce from Proposition 3 another expression of collisional operators $R_1(f_1,f_2)$ and $R_2(f_1,f_2)$:

Proposition 4 *The Boltzmann operators $R_1(f_1,f_2)$ and $R_2(f_1,f_2)$ given by* (48) *and* (55) *are respectively equivalent to the operators*

$$\begin{aligned}R_1(f_1,f_2)(v_1,r)=\frac{2\beta^4}{\pi}(r+r_2)^2\int_{\mathbb{S}^2}\int_{\mathbb{R}^3}\int_{\mathbb{R}^3}&\Big[f_1(v_1',r)f_2(v_2')\exp\left(-\beta^2(v_1-v_2)^2\right)\\&-f_1(v_1,r)f_2(v_2)\exp\left(-\beta^2(v_1'-v_2')^2\right)\Big]\\&\times(n\cdot w)\left[n\cdot(v_1-v_2)\right]1_{\{n\cdot w\geq 0\}}1_{\{n\cdot(v_1-v_2)\geq 0\}}dndwdv_2\end{aligned} \tag{68}$$

with

$$v_1' = \frac{1}{1+\varepsilon(r)}[v_1 + \varepsilon(r)v_2 - \varepsilon(r)w], \tag{69}$$

and

$$\begin{aligned} R_2(f_1,f_2)(v_2) = \frac{2\beta^4}{\pi}\int_{r_{min}}^{r_{max}}\int_{\mathbb{S}^2}\int_{\mathbb{R}^3}\int_{\mathbb{R}^3} \quad & (r+r_2)^2\Big[f_1(v_1',r)f_2(v_2')\exp\left(-\beta^2(v_1-v_2)^2\right) \\ & -f_1(v_1,r)f_2(v_2)\exp\left(-\beta^2(v_1'-v_2')^2\right)\Big] \\ & \times (n\cdot w)\left[n\cdot(v_1-v_2)\right]1_{\{n\cdot w\geq 0\}}1_{\{n\cdot(v_1-v_2)\geq 0\}}drdndwdv_1 \end{aligned} \tag{70}$$

with

$$v_2' = \frac{1}{1+\varepsilon(r)}[v_1 + \varepsilon(r)v_2 + w] \tag{71}$$

where β is given by (46).

Compared to (48) and (55), formulations (68) and (70) are closer to the classical (elastic) multispecies Boltzmann operator obtained by supposing that the kinematic relations of the binary collision are given by (40) instead of (42)(43)(44). The function $\exp(-\beta^2|s|^2)$ in (68) and (70) is a direct consequence of Hypothese 7.

Proof of Proposition 4. Let us start from the expression (65) in which we make the change of variables

$$(v_1, v_2, w) \to (v_1', v_2', v_r)$$

with v_1' and v_2' given by (69)(71) and with $v_r := v_2 - v_1$ (see also (43)). This transformation is involutive, and the inverse transformation is expressed by

$$\left\{\begin{array}{rcl} v_1 &=& \dfrac{1}{1+\varepsilon(r)}[v_1' + \varepsilon(r)v_2' - \varepsilon(r)v_r], \\ v_2 &=& \dfrac{1}{1+\varepsilon(r)}[v_1' + \varepsilon(r)v_2' + v_r], \\ w &=& v_2' - v_1'. \end{array}\right. \tag{72}$$

Then, according to (65), we get

$$\begin{aligned} \int_{\mathbb{R}^3}\varphi(v)R_1^+(f_1,f_2)(v,r)dv = (r+r_2)^2\int_{\mathbb{S}^2}\int_{\mathbb{R}^3}\int_{\mathbb{R}^3}\int_{\mathbb{R}^3} \quad & \varphi(v_1')f_1\left(\frac{v_1'+\varepsilon v_2' - \varepsilon v_r}{1+\varepsilon(r)}, r\right)f_2\left(\frac{v_1'+\varepsilon v_2'+v_r}{1+\varepsilon(r)}\right) \\ & \times h_n(v_2'-v_1')\left[-n\cdot v_r\right]1_{\{-n\cdot v_r\geq 0\}}dndudv_1'dv_2'. \end{aligned} \tag{73}$$

And, by using the involutive character of the transformation $(v_1, v_2, w) \to (v_1', v_2', v_r)$ and by renaming (v_1', v_2', v_r) with (v_1, v_2, w), we deduce from (73) that

$$\begin{aligned} \int_{\mathbb{R}^3}\varphi(v)R_1^+(f_1,f_2)(v,r)dv = (r+r_2)^2\int_{\mathbb{S}^2}\int_{\mathbb{R}^3}\int_{\mathbb{R}^3}\int_{\mathbb{R}^3} \quad & \varphi(v_1)f_1\left(v_1',r\right)f_2\left(v_2'\right) \\ & \times h_n(v_2-v_1)\left(-n\cdot w\right)1_{\{-n\cdot w\geq 0\}}dndwdv_1dv_2. \end{aligned}$$

Using the change of variable $n \to -n$ and the fact that $h_{-n}(s) = h_n(-s)$, we finally obtain that

$$\begin{aligned} \int_{\mathbb{R}^3}\varphi(v)R_1^+(f_1,f_2)(v,r)dv = (r+r_2)^2\int_{\mathbb{S}^2}\int_{\mathbb{R}^3}\int_{\mathbb{R}^3}\int_{\mathbb{R}^3} \quad & \varphi(v_1)f_1\left(v_1',r\right)f_2\left(v_2'\right) \\ & \times h_n(v_1-v_2)\left(n\cdot w\right)1_{\{n\cdot w\geq 0\}}dndwdv_1dv_2. \end{aligned} \tag{74}$$

Thus, by using (67) and (74), we obtain

$$R_1(f_1,f_2)(v,r) = (r+r_2)^2 \int_{\mathbb{S}^2}\int_{\mathbb{R}^3}\int_{\mathbb{R}^3} \quad \big[f_1\left(v_1',r\right) f_2\left(v_2'\right) h_n(v_1-v_2)\left(n\cdot w\right) 1_{\{n\cdot w\geq 0\}} \\ -f_1\left(v_1,r\right) f_2\left(v_2\right) h_n(w)\left[n\cdot(v_1-v_2)\right] 1_{\{n\cdot(v_1-v_2)\geq 0\}}\big] \\ \times dndwdv_2. \tag{75}$$

We finally deduce (68) by using (45). By permuting the subscripts 1 and 2 in (75) and by taking into account an integration in r, we obtain

$$R_2(f_1,f_2)(v) = \int_{r_{min}}^{r_{max}}\int_{\mathbb{S}^2}\int_{\mathbb{R}^3}\int_{\mathbb{R}^3} \quad (r+r_2)^2\big[f_1\left(v_1',r\right) f_2\left(v_2'\right) h_n(v_2-v_1)\left(-n\cdot w\right) 1_{\{-n\cdot w\geq 0\}} \\ -f_1\left(v_1,r\right) f_2\left(v_2\right) h_n(-w)\left[n\cdot(v_2-v_1)\right] 1_{\{n\cdot(v_2-v_1)\geq 0\}}\big] \\ \times drdndwdv_1. \tag{76}$$

Using again the change of variable $n\to -n$ and the fact that $h_{-n}(s)=h_n(-s)$, we deduce from (76) that

$$R_2(f_1,f_2)(v) = \int_{r_{min}}^{r_{max}}\int_{\mathbb{S}^2}\int_{\mathbb{R}^3}\int_{\mathbb{R}^3} \quad (r+r_2)^2\big[f_1\left(v_1',r\right) f_2\left(v_2'\right) h_n(v_1-v_2)\left(n\cdot w\right) 1_{\{n\cdot w\geq 0\}} \\ -f_1\left(v_1,r\right) f_2\left(v_2\right) h_n(w)\left[n\cdot(v_1-v_2)\right] 1_{\{n\cdot(v_1-v_2)\geq 0\}}\big] \\ \times drdndwdv_1. \tag{77}$$

Expression (70) is deduced from (77) by using (45).$\diamondsuit$

4 Derivation of a Vlasov-Boltzmann model

We now introduce another kinetic model which is devoted to approach Boltzmann type model (37) under Hypothesis 3 that is to say when the ratio of mass between a molecule and a dust particle is close to zero. The idea is to use the fact that the velocity of a dust particle after a collision with a molecule is very close to its precollisional velocity (see (61)), like in grazing collisions [21]. In the context of grazing collisions, a Fokker-Plank operator is derived from the classical Boltzmann operator, thanks to an asymptotic expansion with respect to a small parameter (related to the angle of collisions) [21, 1, 19]. Similarly, we propose to perform an asymptotic expansion of the operator $R_1(f_1,f_2)$ with respect to the mass ratio ε defined by (5)(a). This asymptotic analysis will allow us to simplify (in a sense which will be precised) the Boltzmann type operator $R_1(f_1,f_2)$ with a Vlasov type operator. In order to do so, we perform a dimensional analysis of Boltzmann type model (37) which leads to a dimensionless formulation of (37). Let us underline that Hypothesis 4 and 5 allow us to easily introduce this dimensionless formulation of (37).

4.1 Dimensionless formulation of the dust-molecule kinetic model

We now define the dimensionless variables which will be used to derive the dimensionless formulation of the dust-molecule kinetic model (37).

4.1.1 Dimensionless variables

Let us introduce the dimensionless variables $\bar{t}$ and $\bar{x}$

$$\begin{cases} \bar{t} = \dfrac{t}{t^\circ}, & \text{(a)} \\ \\ \bar{x} = \dfrac{x}{L^\circ} & \text{(b)} \end{cases} \tag{78}$$

where t° and L° are characteristic time and length scales which will be chosen in section 5. In order to introduce a unique order of magnitude for the radius r of dust particles, we make this hypothesis:

Hypothesis 8 *We assume that the size of dust particles are of the same order of magnitude. In other words, we have*

$$r_{min} \simeq r_{max}.$$

In the sequel, we denote r° the order of magnitude for the radius of dust particles. We define the dimensionless dust particle radius $\bar{r}$ with

$$\bar{r} = \frac{r}{r^\circ}. \tag{79}$$

Hypothesis 8 allows us to also introduce a unique order of magnitude of the mass of a dust particle – chosen equal to $m_1(r^\circ)$ – and a unique order of magnitude of the dust-molecule collision frequencies ν_{12} and ν_{21} defined by (18)(c,d).

Moreover, we introduce the dimensionless velocities $\hat{v}_1$ and $\check{v}_2$ with

$$\begin{cases} \hat{v}_1 = \dfrac{v_1}{V_1^\circ}, \\ \\ \check{v}_2 = \dfrac{v_2}{V_2^\circ} \end{cases} \tag{80}$$

where V_1° and V_2° are velocity scales. For the sake of simplicity, we use the notation

$$\delta := \frac{V_1^\circ}{V_2^\circ}.$$

We propose two different velocity scalings:

- In the first scaling, we choose

$$\begin{cases} V_1^\circ =< V_1 >:= \sqrt{\dfrac{8kT^\circ}{\pi m_1(r^\circ)}}, \\ \\ V_2^\circ =< V_2 >:= \sqrt{\dfrac{8kT^\circ}{\pi m_2}} \end{cases} \tag{81}$$

  where T° has been introduced in Hypothesis 5. Thus, we have

$$V_1^\circ = \sqrt{\varepsilon}\, V_2^\circ \ll V_2^\circ, \tag{82}$$

  where

$$\varepsilon := \varepsilon(r^\circ), \tag{83}$$

  that is to say

$$\delta = \sqrt{\varepsilon} \ll 1$$

  because of Hypothesis 3 for this first scaling. Thanks to Hypothesis 5 and 8, $< V_1 >$ and $< V_2 >$ given by (81) are respectively characteristic thermal velocities of dust particles and of gas molecules. Such velocity scales have been already used for a disparate mass binary gas in [16, 17, 18] to study the epochal relaxation phenomenon [30]. However, on the contrary to [16, 17, 18], neither cross sections (because of Hypothesis 2) nor densities (because of Hypothesis 4) are in our context of the same order of magnitude.

- In the second scaling, we introduce a unique order of magnitude V° for the velocity scales V_1° and V_2° that is to say

$$\begin{cases} V_1^\circ := V^\circ, \\ \\ V_2^\circ := V^\circ. \end{cases} \tag{84}$$

Thus, we have

$$\delta = 1.$$

We can choose for example $V^\circ =< V_2 >$. In fact, the *exact* choice of V° is not really important to formally derive the Vlasov operator. Nevertheless, the fact that $\delta = 1$ instead of $\delta = \sqrt{\varepsilon}$ is important to estimate the error introduced by the Vlasov operator.

At last, we introduce the dimensionless densities $\hat{f}_1$ and $\check{f}_2$ in the phase space

$$\left\{ \begin{array}{l} \hat{f}_1(\bar{t},\bar{x},\hat{v}_1,\bar{r}) = \dfrac{\left(V_1^\circ\right)^3 r^\circ}{n_1^\circ}\, f_1(t,x,v,r), \\ \\ \check{f}_2(\bar{t},\bar{x},\check{v}_2) = \dfrac{\left(V_2^\circ\right)^3}{n_2^\circ}\, f_2(t,x,v_2). \end{array} \right. \tag{85}$$

By using (79) and (80), we deduce from (85) that

$$n_1^\circ \hat{f}_1 d\hat{v}_1 d\bar{r} = f_1 dv_1 dr \qquad \text{and} \qquad n_2^\circ \check{f}_2 d\check{v}_2 = f_2 dv_2.$$

As a consequence, we have

$$\sup_{\bar{\Omega}} \int_{\mathbb{R}^3} \int_{\bar{r}_{min}}^{\bar{r}_{max}} \hat{f}_1 d\hat{v}_1 d\bar{r} = \mathcal{O}(1) \qquad \text{and} \qquad \inf_{\bar{\Omega}} \int_{\mathbb{R}^3} \check{f}_2 d\check{v}_2 = \mathcal{O}(1)$$

at the beginning of a LOVA in ITER by using Hypothesis 4 (see (12)), where $\bar{r}_{min} = r_{min}/r^\circ$, $\bar{r}_{max} = r_{max}/r^\circ$ and $\bar{\Omega}$ being deduced from Ω through scaling (78)(b).

4.1.2 Dimensionless kinetic model

By using the dimensionless variables $(\bar{t},\bar{x},\bar{r},\hat{v}_1,\check{v}_2)$ defined with (78), (79) and (80), and the dimensionless densities $\hat{f}_1$ and $\check{f}_2$ defined with (85), the dimensionless formulation of system (37) is given by

$$\left\{ \begin{array}{l} \dfrac{\partial \hat{f}_1}{\partial \bar{t}} + \dfrac{V_1^\circ t^\circ}{L^\circ}\, \hat{v}_1 \cdot \nabla_{\bar{x}} \hat{f}_1 = t^\circ n_2^\circ (r^\circ)^2 V_2^\circ\, \bar{R}_1(\hat{f}_1,\check{f}_2)(\bar{t},\bar{x},\hat{v}_1,\bar{r}), \\ \\ \dfrac{\partial \check{f}_2}{\partial \bar{t}} + \dfrac{V_2^\circ t^\circ}{L^\circ}\, \check{v}_2 \cdot \nabla_{\bar{x}} \check{f}_2 = t^\circ n_1^\circ (r^\circ)^2 V_2^\circ\, \bar{R}_2(\hat{f}_1,\check{f}_2) + t^\circ n_2^\circ V_2^\circ r_2^2\, \bar{Q}(\check{f}_2,\check{f}_2). \end{array} \right. \tag{86}$$

Here, $\bar{Q}(\check{f}_2,\check{f}_2)$ is defined by

$$\bar{Q}(\check{f}_2,\check{f}_2)(\bar{t},\bar{x},\check{v}) = \int_{\mathbb{S}^2} \int_{\mathbb{R}^3} \left[\check{f}_2(\bar{t},\bar{x},\check{v}'_*)\check{f}_2(\bar{t},\bar{x},\check{v}'_*) - \check{f}_2(\bar{t},\bar{x},\check{v})\check{f}_2(\bar{t},\bar{x},\check{v}_*) \right] |\check{v}-\check{v}_*| d\sigma d\check{v}_* \tag{87}$$

where

$$\left\{ \begin{array}{rcl} \check{v}' & = & \dfrac{\check{v}+\check{v}_*}{2} + \dfrac{|\check{v}-\check{v}_*|}{2}\sigma, \\ \\ \check{v}'_* & = & \dfrac{\check{v}+\check{v}_*}{2} - \dfrac{|\check{v}-\check{v}_*|}{2}\sigma. \end{array} \right.$$

The dimensionless operator $\bar{R}_1(\hat{f}_1,\check{f}_2)$ deduced from (68) is defined by

$$\begin{array}{rl} \bar{R}_1(\hat{f}_1,\check{f}_2)(\bar{t},\bar{x},\hat{v}_1,\bar{r}) = \dfrac{2\bar{\beta}^4}{\pi} \left[\bar{r} + \left(\dfrac{\varepsilon}{\eta}\right)^{1/3} \right]^2 \displaystyle\int_{\mathbb{S}^2} \int_{\mathbb{R}^3} \int_{\mathbb{R}^3} & \Big[\hat{f}_1(\bar{t},\bar{x},\hat{v}'_1,\bar{r})\check{f}_2(\bar{t},\bar{x},\check{v}'_2) \exp\left(-\bar{\beta}^2(\delta\hat{v}_1 - \check{v}_2)^2\right) \\ & -\hat{f}_1(\bar{t},\bar{x},\hat{v}_1,\bar{r})\check{f}_2(\bar{t},\bar{x},\check{v}_2) \exp\left(-\bar{\beta}^2\check{w}\right) \Big] \\ & \times (n\cdot\check{w})\left[n\cdot(\delta\hat{v}_1-\check{v}_2)\right] 1_{\{n\cdot\check{w}\geq 0\}} 1_{\{n\cdot(\delta\hat{v}_1-\check{v}_2)\geq 0\}} \\ & \times dn d\check{w} d\check{v}_2 \end{array} \tag{88}$$

where

$$\hat{v}_1' = \frac{1}{1+\varepsilon\bar{r}^{-3}}\left(\hat{v}_1 + \frac{\varepsilon}{\delta}\bar{r}^{-3}\,\check{v}_2 - \frac{\varepsilon}{\delta}\bar{r}^{-3}\,\check{w}\right) \tag{89}$$

is the dimensionless formulation of (69), $\check{w}$ being the dimensionless velocity

$$\check{w} = \frac{w}{V_2^\circ}$$

and $\bar{\beta}$ being the dimensionless constant

$$\bar{\beta} := V_2^\circ \beta = \sqrt{\frac{4T^\circ}{\pi T_{surf}}} \cdot \frac{V_2^\circ}{< V_2 >}$$

where the thermal velocity $1/\beta$ is given by (46). In the same way, the dimensionless operator $\bar{R}_2(\hat{f}_1, \check{f}_2)$ deduced from (70) and (71) is defined by

$$\begin{aligned}\bar{R}_2(\hat{f}_1,\check{f}_2)(\bar{t},\bar{x},\check{v}_2) = \frac{2\bar{\beta}^4}{\pi}\int_{\bar{r}_{min}}^{\bar{r}_{max}}\int_{\mathbb{S}^2}\int_{\mathbb{R}^3}\int_{\mathbb{R}^3} & \left[\bar{r}+\left(\frac{\varepsilon}{\eta}\right)^{1/3}\right]^2\left[\hat{f}_1(\bar{t},\bar{x},\hat{v}_1',\bar{r})\check{f}_2(\bar{t},\bar{x},\check{v}_2')\exp\left(-\bar{\beta}^2(\delta\hat{v}_1-\check{v}_2)^2\right)\right.\\ & \left.-\hat{f}_1(\bar{t},\bar{x},\hat{v}_1,\bar{r})\check{f}_2(\bar{t},\bar{x},\check{v}_2)\exp\left(-\bar{\beta}^2\check{w}^2\right)\right]\\ & \times(n\cdot\check{w})\left[n\cdot(\delta\hat{v}_1-\check{v}_2)\right]1_{\{n\cdot\check{w}\geq 0\}}1_{\{n\cdot(\delta\hat{v}_1-\check{v}_2)\geq 0\}}\\ & \times d\bar{r}dnd\check{w}d\hat{v}_1\end{aligned} \tag{90}$$

with

$$\check{v}_2' = \frac{1}{1+\varepsilon\bar{r}^{-3}}\left(\delta\,\hat{v}_1 + \varepsilon\bar{r}^{-3}\,\check{v}_2 + \check{w}\right). \tag{91}$$

Let us note that we have replaced $\frac{r_2}{r^\circ}$ by $\left(\frac{\varepsilon}{\eta}\right)^{1/3}$ in (88) and (90) by using relation (8), and that, under Hypothesis 8, we have $\bar{r}_{min} = \mathcal{O}(1)$ and $\bar{r}_{max} = \mathcal{O}(1)$ in (90).

4.2 Asymptotic expansion of dust-molecule kinetic operator $R_1(f_1, f_2)$

To approximate $R_1(f_1, f_2)$ with a Vlasov type operator, we perform an asymptotic expansion to the dimensionless weak operator $\bar{R}_1(\hat{f}_1, \check{f}_2)$ defined by (86) with respect to the ratio of mass between a gas molecule and a dust particle:

Proposition 5 *Let φ be a test function ($\varphi \in \mathcal{C}_c^0(\mathbb{R}^3)$ for example), let $R_1(f_1, f_2)$ be the dimensionless Boltzmann type operator* (88)*. Then, we have formally*

$$\int_{\mathbb{R}^3}\varphi(\hat{v}_1)\bar{R}_1(\hat{f}_1,\check{f}_2)(\bar{t},\bar{x},\hat{v}_1,\bar{r})d\hat{v}_1 = \frac{\varepsilon}{\delta}\int_{\mathbb{R}^3}\bar{\Upsilon}(\check{f}_2)(\bar{t},\bar{x},\hat{v}_1,\bar{r})\cdot\nabla\varphi(\hat{v}_1)\hat{f}_1(\bar{t},\bar{x},\hat{v}_1,\bar{r})d\hat{v}_1 + o\left(\frac{\varepsilon}{\delta}\right) \tag{92}$$

where $\bar{\Upsilon}(\check{f}_2)(\bar{t},\bar{x},\bar{r})$ is given by

$$\bar{\Upsilon}_a(\check{f}_2)(\bar{t},\bar{x},\bar{r}) = \frac{\pi}{\bar{r}}\int_{\mathbb{R}^3}\check{f}_2(\bar{t},\bar{x},\check{v}_2)\left[|\check{v}_2| + \frac{\sqrt{\pi}}{3\bar{\beta}}\right]\check{v}_2 d\check{v}_2 \tag{93}$$

in the case of first scaling (81) (i.e. $\delta = \sqrt{\varepsilon}$), and by

$$\bar{\Upsilon}_b(\check{f}_2)(\bar{t},\bar{x},\hat{v}_1,\bar{r}) = \frac{\pi}{\bar{r}}\int_{\mathbb{R}^3}\check{f}_2(\bar{t},\bar{x},\check{v}_2)\left[|\check{v}_2-\hat{v}_1| + \frac{\sqrt{\pi}}{3\bar{\beta}}\right](\check{v}_2-\hat{v}_1)d\check{v}_2 \tag{94}$$

in the case of second scaling (84) (i.e. $\delta = 1$).

We deduce from Proposition 5:

Proposition 6 *Let $R_1(f_1, f_2)$ be the dimensionless Boltzmann type operator* (88)*. Then, we have formally*

$$\bar{R}_1(\hat{f}_1, \check{f}_2)(\bar{t}, \bar{x}, \hat{v}_1, \bar{r}) = -\sqrt{\varepsilon}\ \bar{\Upsilon}_a(\check{f}_2)(\bar{t}, \bar{x}, \bar{r}) \cdot \nabla_{\hat{v}_1}[\hat{f}_1(\bar{t}, \bar{x}, \hat{v}_1, \bar{r})] + o\left(\sqrt{\varepsilon}\right) \tag{95}$$

in the case of first scaling (81), and

$$\bar{R}_1(\hat{f}_1, \check{f}_2)(\bar{t}, \bar{x}, \hat{v}_1, \bar{r}) = -\varepsilon\ \nabla_{\hat{v}_1} \cdot [\bar{\Upsilon}_b(\check{f}_2)(\bar{t}, \bar{x}, \hat{v}_1, \bar{r})\hat{f}_1(\bar{t}, \bar{x}, \hat{v}_1, \bar{r})] + o\left(\varepsilon\right) \tag{96}$$

in the case of second scaling (84), $\bar{\Upsilon}_a(\check{f}_2)$ and $\bar{\Upsilon}_b(\check{f}_2)$ being respectively given by (93) and by (94).

Proof of Proposition 5. We easily deduce from the weak formulation (57) of $R_1(f_1, f_2)$ and from the dimensionless formulation (88) of $R_1(f_1, f_2)$ that the dimensionless weak formulation of $\bar{R}_1(\hat{f}_1, \check{f}_2)$ is given by

$$\begin{aligned}
&\int_{\mathbb{R}^3} \bar{R}_1(\hat{f}_1, \check{f}_2)(\bar{t}, \bar{x}, \hat{v}_1, \bar{r})\varphi(\hat{v}_1)d\hat{v}_1 \\
&= \frac{2\bar{\beta}^4}{\pi}\left(\bar{r} + \left(\frac{\varepsilon}{\eta}\right)^{1/3}\right)^2 \int_{\mathbb{S}^2}\int_{\mathbb{R}^3}\int_{\mathbb{R}^3}\int_{\mathbb{R}^3} \left[\varphi(\hat{v}_1') - \varphi(\hat{v}_1)\right] \hat{f}_1(\bar{t}, \bar{x}, \hat{v}_1, \bar{r})\check{f}_2(\bar{t}, \bar{x}, \check{v}_2) \\
&\quad \times \exp\left(-\bar{\beta}^2\check{w}^2\right)(n \cdot \check{w})\left[n \cdot (\delta\hat{v}_1 - \check{v}_2)\right] 1_{\{n\cdot\check{w}\geq 0\}} 1_{\{n\cdot(\delta\hat{v}_1 - \check{v}_2)\geq 0\}} dn d\check{w} d\hat{v}_1 d\check{v}_2
\end{aligned}$$

where $\hat{v}_1'$ given by (89) is the dimensionless formulation of (69). Since

$$\begin{aligned}
\hat{v}_1' - \hat{v}_1 &= \frac{1}{1 + \varepsilon\bar{r}^{-3}}\left(-\varepsilon\bar{r}^{-3}\,\hat{v}_1 + \frac{\varepsilon}{\delta}\bar{r}^{-3}\,\check{v}_2 - \frac{\varepsilon}{\delta}\bar{r}^{-3}\,\check{w}\right) \\
&= \mathcal{O}(\sqrt{\varepsilon}) \quad \text{if } \delta = \sqrt{\varepsilon}, \\
&= \mathcal{O}(\varepsilon) \quad \text{if } \delta = 1,
\end{aligned}$$

we can make an asymptotic expansion of $\varphi(\hat{v}_1') - \varphi(\hat{v}_1)$ at the first order of $\frac{\varepsilon}{\delta}$, that is to say

$$\begin{aligned}
\varphi(\hat{v}_1') - \varphi(\hat{v}_1) &= (\hat{v}_1' - \hat{v}_1) \cdot \nabla\varphi\left(\hat{v}_1\right) + \mathcal{O}\left(\left|\hat{v}_1' - \hat{v}_1\right|^2\right) \\
&= \frac{\varepsilon}{\delta}\bar{r}^{-3}\left(\check{v}_2 - w - \delta\hat{v}_1\right) \cdot \nabla\varphi\left(\hat{v}_1\right) + \mathcal{O}\left(\frac{\varepsilon^2}{\delta^2}\right).
\end{aligned} \tag{97}$$

Thus, we obtain at least formally

$$\begin{aligned}
&\int_{\mathbb{R}^3} \bar{R}_1(\hat{f}_1, \check{f}_2)(\bar{t}, \bar{x}, \hat{v}_1, \bar{r})\varphi(\hat{v}_1)d\hat{v}_1 \\
&= \frac{\varepsilon}{\delta} \cdot \frac{2\bar{\beta}^4}{\pi\bar{r}} \int_{\mathbb{R}^3}\int_{\mathbb{R}^3} \hat{f}_1(\bar{t}, \bar{x}, \hat{v}_1, \bar{r})\check{f}_2(\bar{t}, \bar{x}, \check{v}_2)\nabla\varphi\left(\hat{v}_1\right) \cdot \left[I(\hat{v}_1, \check{v}_2) - J(\hat{v}_1, \check{v}_2)\right] d\hat{v}_1 d\check{v}_2 + o\left(\frac{\varepsilon}{\delta}\right)
\end{aligned}$$

where

$$I(\hat{v}_1, \check{v}_2) = (\check{v}_2 - \delta\hat{v}_1)\int_{\mathbb{S}^2}\left[n \cdot (\delta\hat{v}_1 - \check{v}_2)\right] 1_{\{n\cdot(\delta\hat{v}_1 - \check{v}_2)\geq 0\}}\left[\int_{\mathbb{R}^3} \exp\left(-\bar{\beta}^2\check{w}^2\right)(n \cdot \check{w})\, 1_{\{n\cdot\check{w}\geq 0\}} d\check{w}\right] dn,$$

and

$$J(\hat{v}_1, \check{v}_2) = \int_{\mathbb{S}^2}\left[n \cdot (\delta\hat{v}_1 - \check{v}_2)\right] 1_{\{n\cdot(\delta\hat{v}_1 - \check{v}_2)\geq 0\}}\left[\int_{\mathbb{R}^3} \exp\left(-\bar{\beta}^2\check{w}^2\right)(n \cdot \check{w})\,\check{w} 1_{\{n\cdot\check{w}\geq 0\}} d\check{w}\right] dn.$$

Moreover, by using (47), we obtain

$$\forall n \in \mathbb{S}^2 : \quad \int_{\mathbb{R}^3} \exp\left(-\bar{\beta}^2\check{w}^2\right)(n \cdot \check{w})\, 1_{\{n\cdot\check{w}\geq 0\}} d\check{w} = \frac{\pi}{2\bar{\beta}^4}. \tag{98}$$

We have also [11]

$$\forall n \in \mathbb{S}^2 : \quad \int_{\mathbb{R}^3} \exp\left(-\bar{\beta}^2 \check{w}^2\right)(n \cdot \check{w})\, \check{w} 1_{\{n\cdot\check{w}\geq 0\}} d\check{w} = \frac{\pi^{3/2}}{4\bar{\beta}^5} n \tag{99}$$

and

$$\forall k \in \mathbb{R}^3 : \quad \int_{\mathbb{S}^2} n(n \cdot k) 1_{\{n\cdot k\geq 0\}} dn = \frac{2\pi}{3} k. \tag{100}$$

Then, thanks to (66), (98), (99) and (100), we obtain

$$I(\hat{v}_1, \check{v}_2) = \frac{\pi^2}{2\bar{\beta}^4}\ |\check{v}_2 - \delta\hat{v}_1|\,(\check{v}_2 - \delta\hat{v}_1)$$

and

$$J(\hat{v}_1, \check{v}_2) = \frac{\pi^{5/2}}{6\bar{\beta}^5}\ (\delta\hat{v}_1 - \check{v}_2)\,.$$

Finally, we obtain for $\delta = \sqrt{\varepsilon}$

$$\begin{aligned}
&\int_{\mathbb{R}^3} \bar{R}_1(\hat{f}_1, \check{f}_2)(\bar{t}, \bar{x}, \hat{v}_1, \bar{r})\varphi(\hat{v}_1) d\hat{v}_1 \\
&= \frac{\pi}{\bar{r}}\sqrt{\varepsilon} \iint_{\mathbb{R}^3\times\mathbb{R}^3} \hat{f}_1(\bar{t}, \bar{x}, \hat{v}_1, \bar{r})\check{f}_2(\bar{t}, \bar{x}, \check{v}_2)\nabla\varphi\,(\hat{v}_1)\cdot\check{v}_2 \left[|\check{v}_2| + \frac{\sqrt{\pi}}{3\bar{\beta}}\right] d\check{v}_2 d\hat{v}_1 + o(\sqrt{\varepsilon}),
\end{aligned}$$

and for $\delta = 1$

$$\begin{aligned}
&\int_{\mathbb{R}^3} \bar{R}_1(\hat{f}_1, \check{f}_2)(\bar{t}, \bar{x}, \hat{v}_1, \bar{r})\varphi(\hat{v}_1) d\hat{v}_1 \\
&= \frac{\pi}{\bar{r}}\varepsilon \iint_{\mathbb{R}^3\times\mathbb{R}^3} \hat{f}_1(\bar{t}, \bar{x}, \hat{v}_1, \bar{r})\check{f}_2(\bar{t}, \bar{x}, \check{v}_2)\nabla\varphi\,(\hat{v}_1)\cdot(\check{v}_2 - \hat{v}_1) \left[|\check{v}_2 - \hat{v}_1| + \frac{\sqrt{\pi}}{3\bar{\beta}}\right] d\check{v}_2 d\hat{v}_1 + o(\varepsilon),
\end{aligned}$$

which gives (92) , (93) and (94).$\diamondsuit$

4.3 The Vlasov-Boltzmann model

By using Proposition 6, we are able to approximate Boltzmann type system (37) with a Vlasov-Boltzmann type system.

4.3.1 The dimensionless Vlasov-Boltzmann model

We deduce from Proposition 6 that dimensionless Boltzmann type model (86) is such that

$$\begin{cases}
\dfrac{\partial \hat{f}_1}{\partial \bar{t}} + \dfrac{V_1^\circ t^\circ}{L^\circ}\,\hat{v}_1\cdot\nabla_{\bar{x}}\hat{f}_1 + \dfrac{\varepsilon}{\delta} t^\circ n_2^\circ (r^\circ)^2 V_2^\circ \nabla_{\hat{v}_1}\cdot[\bar{\Upsilon}(\check{f}_2)(\bar{t}, \bar{x}, \hat{v}_1, \bar{r})\hat{f}_1(\bar{t}, \bar{x}, \hat{v}_1, \bar{r})] = o\left(\dfrac{\varepsilon}{\delta}\right), \\
\dfrac{\partial \check{f}_2}{\partial \bar{t}} + \dfrac{V_2^\circ t^\circ}{L^\circ}\,\check{v}_2\cdot\nabla_{\bar{x}}\check{f}_2 = t^\circ n_1^\circ (r^\circ)^2 V_2^\circ\, \bar{R}_2(\hat{f}_1, \check{f}_2) + t^\circ n_2^\circ V_2^\circ r_2^2\, \bar{Q}(\check{f}_2, \check{f}_2)
\end{cases} \tag{101}$$

where $\bar{R}_2(\hat{f}_1, \check{f}_2)$ and $\bar{Q}(\check{f}_2, \check{f}_2)$ are respectively given by (87) and (90), where $\delta \in \{1, \sqrt{\varepsilon}\}$, and where $\bar{\Upsilon}(\check{f}_2)$ is given by (93) for the first scaling (81) (*i.e.* $\delta = \sqrt{\varepsilon}$) and by (94) for the second scaling (84) (*i.e.* $\delta = 1$).

4.3.2 The Vlasov-Boltzmann model

We deduce from Proposition 6 that:

Corollary 1 *Let $R_1(f_1, f_2)$ be the Boltzmann type operator (68). Then, we have formally*

$$R_1(f_1, f_2)(t, x, v_1, r) = -\Upsilon_a(f_2)(t, x, r)\cdot\nabla_{v_1}[f_1(t, x, v_1, r)] + o\left(\sqrt{\varepsilon}\right) \tag{102}$$

in the case of first scaling (81), and

$$R_1(f_1,f_2)(t,x,v_1,r) = -\nabla_{v_1}\cdot[\Upsilon_b(f_2)(t,x,v_1,r)f_1(t,x,v_1,r)] + o(\varepsilon) \tag{103}$$

in the case of second scaling (84), $\Upsilon_a(f_2)$ and $\Upsilon_b(f_2)$ being given by

$$\begin{cases} \Upsilon_a(f_2)(t,x,r) = \pi\varepsilon\dfrac{(r^\circ)^3}{r}\displaystyle\int_{\mathbb{R}^3} f_2(t,x,v_2)\left[|v_2| + \frac{\sqrt{\pi}}{3\beta}\right]v_2 dv_2, & (a) \\ \Upsilon_b(f_2)(t,x,v_1,r) = \pi\varepsilon\dfrac{(r^\circ)^3}{r}\displaystyle\int_{\mathbb{R}^3} f_2(t,x,v_2)\left[|v_2-v_1| + \frac{\sqrt{\pi}}{3\beta}\right](v_2-v_1) dv_2. & (b) \end{cases} \tag{104}$$

Operators (102) and (103) are Vlasov type operators.

As a consequence, the Vlasov-Boltzmann model

$$\begin{cases} \dfrac{\partial f_1}{\partial t} + v\cdot\nabla_x f_1 + \Upsilon_a(f_2)(t,x,r)\cdot\nabla_v f_1(t,x,v,r) = 0, & \text{(a)} \\ \dfrac{\partial f_2}{\partial t} + v\cdot\nabla_x f_2 = R_2(f_1,f_2) + Q(f_2,f_2), & \text{(b)} \\ (t,x,v,r)\in\mathbb{R}^+\times\Omega\times\mathbb{R}^3\times[r_{min},r_{max}] \end{cases} \tag{105}$$

where $\Upsilon_a(f_2)$ is given by (104)(a) equals Boltzmann type model (37) to error $o(\sqrt{\varepsilon})$. And, the Vlasov-Boltzmann model

$$\begin{cases} \dfrac{\partial f_1}{\partial t} + v\cdot\nabla_x f_1 + \nabla_v\cdot[\Upsilon_b(f_2)(t,x,v,r)f_1(t,x,v,r)] = 0, & \text{(a)} \\ \dfrac{\partial f_2}{\partial t} + v\cdot\nabla_x f_2 = R_2(f_1,f_2) + Q(f_2,f_2), & \text{(b)} \\ (t,x,v,r)\in\mathbb{R}^+\times\Omega\times\mathbb{R}^3\times[r_{min},r_{max}] \end{cases} \tag{106}$$

where $\Upsilon_b(f_2)$ is given by (104)(b) equals Boltzmann type model (37) to error $o(\varepsilon)$. System (106) is certainly a best approximation of (37) than system (105). Nevertheless, it is more expensive to solve system (106) than system (105) because $\Upsilon_b(f_2)$ is a function of v_1 which is not the case of $\Upsilon_a(f_2)$. We will justify these assertions in Section 6.

At last, let us underline that $m_1\Upsilon_a(f_2)$ and $m_1\Upsilon_b(f_2)$ define two drag force models for the dust particles which are also valid when the gas molecules are not at thermodynamical equilibrium in the sense that they depend on f_2 through (104)(a) and (104)(b). Moreover, these drag forces do not depend on empirical coefficients thanks to (104), which is not the case for other drag forces especially adapted in a rarefied atmosphere as in [3].

5 Study of the Vlasov-Boltzmann model at different time and length scales

To estimate the appropriate characteristic time scale t° and the appropriate characteristic length scale L° in the case of the beginning of a LOVA in ITER, we propose in this section a brief qualitative analysis of system (105) obtained, under Hypothesis 8, with first velocity scaling (81). The dimensionless formulation of this Vlasov-Boltzmann system is given by (see (101) with $\delta = \sqrt{\varepsilon}$)

$$\begin{cases} \dfrac{\partial \hat{f}_1}{\partial \bar{t}} + \dfrac{< V_1 > t^\circ}{L^\circ}\,\hat{v}_1\cdot\nabla_{\bar{x}}\hat{f}_1 + \sqrt{\varepsilon}\; t^\circ n_2^\circ (r^\circ)^2 < V_2 > \bar{\Upsilon}_a(\check{f}_2)(\bar{t},\bar{x},\bar{r})\cdot\nabla_{\hat{v}_1}\hat{f}_1 = 0, \\ \dfrac{\partial \check{f}_2}{\partial \bar{t}} + \dfrac{< V_2 > t^\circ}{L^\circ}\,\check{v}_2\cdot\nabla_{\bar{x}}\check{f}_2 = t^\circ n_1^\circ (r^\circ)^2 < V_2 > \bar{R}_2(\hat{f}_1,\check{f}_2) + t^\circ n_2^\circ < V_2 > r_2^2\,\bar{Q}(\check{f}_2,\check{f}_2) \end{cases} \tag{107}$$

where $\bar{\Upsilon}_a(\check{f}_2)(\bar{t},\bar{x},\bar{r})$ is given by (93). Let us underline that we could also lead this qualitative analysis with the second velocity scaling (84) which gives in particular, instead of $\bar{\Upsilon}_a(\check{f}_2)(\bar{t},\bar{x},\bar{r})$, the more precise Vlasov operator $\bar{\Upsilon}_b(\check{f}_2)(\bar{t},\bar{x},\hat{v}_1,\bar{r})$ defined by (94). Nevertheless, this would not give more qualitative informations about t° and L°. To simplify the qualitative analysis, we suppose:

Hypothesis 9 *We assume that the parameters α°, r° and r_2 are such that*

$$\frac{1}{4\sqrt{2}}\alpha^\circ\left(\frac{r^\circ}{r_2}\right)^2 \simeq 1. \tag{108}$$

Hypothesis 10 *We assume that the parameters ε, r° and r_2 are such that*

$$\frac{\sqrt{\varepsilon}}{4\sqrt{2}}\left(\frac{r^\circ}{r_2}\right)^2 \simeq 1, \tag{109}$$

that is to say

$$\frac{1}{4\sqrt{2}}\left(\eta\frac{r^\circ}{r_2}\right)^{1/2} \simeq 1, \tag{110}$$

where η is given by (7).

Relations (108) and (109) are verified for the orders of magnitude introduced in (17).

5.1 Definition of the characteristic time scale t°

Under Hypothesis 1-8 (see also section 2.2.1), we can introduce the following three characteristic time scales

$$\left\{\begin{array}{ll} t_{22} = \left(4\sqrt{2}\pi\, r_2^2\, n_2^\circ\, < V_2 >\right)^{-1}, & \text{(a)} \\ \\ t_{12} = \left(\pi\,(r^\circ)^2\, n_2^\circ\, < V_2 >\right)^{-1}, & \text{(b)} \\ \\ t_{21} = \left(\pi\,(r^\circ)^2\, n_1^\circ\, < V_2 >\right)^{-1} & \text{(c)} \end{array}\right. \tag{111}$$

relative to the dust-molecule mixture. By using (19) and by noting that $< V_2 >=< V_{22}^{rel} > /\sqrt{2}$ and that $< V_2 >\simeq< V_{12}^{rel} >=< V_{21}^{rel} >$, we obtain that these three characteristic time scales are approximately equal to the mean collision times introduced in (18)(b,c,d) for the radius $r = r^\circ$. We can notice that we have

$$t_{12} = \alpha^\circ\, t_{21} \ll t_{21} \tag{112}$$

(see also (20)(c) and (25)(a)). Moreover, under Hypothesis 8 and 9, we get $t_{21} \simeq t_{22}$, which implies that

$$t_{12} \ll t_{21} \simeq t_{22} \tag{113}$$

by also using (112). This allows us to considere only two characteristic time scales in our qualitative analysis: the characteristic time scale t_{22} relative to collisions between molecules, and the characteristic time scale t_{12} relative to collisions between dust particles and gas molecules (from the point of view of dust particles) which is the smaller of these two time scales.

5.2 Definition of the characteristic length scale L°

We define the characteristic length scale L° from the time scale $t^\circ \in \{t_{12}, t_{22}\}$ as the mean distance covered by one of the two species during the time t°. Then, for each time scale t°, we can considere two different length scales L_1 and L_2, which correspond to the mean distance covered by dust particles and molecules respectively :

$$\textit{when we choose}\quad t^\circ = t_{12}: \quad \left\{\begin{array}{lll} L_1 := t_{12} < V_1 > & \Longrightarrow & L_1 = \lambda_{12}, \quad \text{(a)} \\ \\ L_2 := t_{12} < V_2 > & \Longrightarrow & L_2 = \dfrac{\lambda_{12}}{\sqrt{\varepsilon}} \quad \text{(b)} \end{array}\right. \tag{114}$$

and

$$\textit{when we choose} \quad t^\circ = t_{22} : \quad \left\{ \begin{array}{lll} L_1 := t_{22} < V_1 > & \Longrightarrow & L_1 = \sqrt{\varepsilon}\ \lambda_{22}, \quad \text{(a)} \\ \\ L_2 := t_{22} < V_2 > & \Longrightarrow & L_2 = \lambda_{22} \qquad \text{(b)} \end{array} \right. \tag{115}$$

where $\lambda_{ij} =< V_i > t_{ij}$ is the mean free path of the collision of a particle of type i with a particle of type j *from the point of view of the particle of type* i (see also section 2.2.2). We recall that under Hypothesis 8 and 9, we have (see (29))

$$\lambda_{22} \simeq \lambda_{21} \tag{116}$$

which allows us to only consider the two characteristic length scales λ_{12} and λ_{22}. Nevertheless, for the sake of completness, we also study the two characteristic length scales $\lambda_{12}/\sqrt{\varepsilon}$ and $\sqrt{\varepsilon}\ \lambda_{22}$ since these length scales are deduced from the choice of the velocity scale $V^\circ \in \{< V_1 >, < V_2 >\}$ in (114)(b) and (115)(a). Moreover, under Hypothesis 8–10, we deduce from (27)(b) that

$$\left\{ \begin{array}{l} \dfrac{\lambda_{12}}{\lambda_{22}} \simeq \sqrt{\varepsilon}\ \alpha^\circ, \\ \\ \dfrac{\lambda_{12}/\sqrt{\varepsilon}}{\lambda_{22}\sqrt{\varepsilon}} \simeq \dfrac{4\sqrt{2}}{\sqrt{\varepsilon}} \left(\dfrac{r_2}{r^\circ}\right)^2 \simeq 1. \end{array} \right.$$

As a consequence, the four characteristic length scales defined in (114) and (115) are such that

$$\lambda_{12} \ll \frac{\lambda_{12}}{\sqrt{\varepsilon}} \simeq \sqrt{\varepsilon}\ \lambda_{22} \ll \lambda_{22} \tag{117}$$

under Hypothesis 8–10.

5.3 The Vlasov-Boltzmann model when $t^\circ = t_{12}$ and $L^\circ = \lambda_{12}$

We considere the time and space scales defined by (111)(b) and (114)(a). These scales are the smallest ones that we can define in the dust-molecule mixture (see (113) and (117)). In that case, system (107) is given by

$$\left\{ \begin{array}{l} \dfrac{\partial \hat{f}_1}{\partial \bar{t}} + \hat{v}_1 \cdot \nabla_{\bar{x}} \hat{f}_1 + \dfrac{\sqrt{\varepsilon}}{\pi}\ \bar{\Upsilon}_a(\check{f}_2)(\bar{t}, \bar{x}, \hat{v}_1, \bar{r}) \cdot \nabla_{\hat{v}_1} \hat{f}_1 = 0, \qquad \text{(a)} \\ \\ \dfrac{\partial \check{f}_2}{\partial \bar{t}} + \dfrac{1}{\sqrt{\varepsilon}} \check{v}_2 \cdot \nabla_{\bar{x}} \check{f}_2 = \dfrac{\alpha^\circ}{\pi} \bar{R}_2(\hat{f}_1, \check{f}_2) + \dfrac{1}{\pi} \left(\dfrac{r_2}{r^\circ}\right)^2 \bar{Q}(\check{f}_2, \check{f}_2). \quad \text{(b)} \end{array} \right. \tag{118}$$

Thanks to Hypothesis 2-4, we notice that system (118) is close to

$$\left\{ \begin{array}{l} \dfrac{\partial \hat{f}_1}{\partial \bar{t}} + \hat{v}_1 \cdot \nabla_{\bar{x}} \hat{f}_1 = 0, \qquad \text{(a)} \\ \\ \dfrac{\partial \check{f}_2}{\partial \bar{t}} + \dfrac{1}{\sqrt{\varepsilon}} \check{v}_2 \cdot \nabla_{\bar{x}} \check{f}_2 = 0. \quad \text{(b)} \end{array} \right. \tag{119}$$

As a consequence, the choice $(t^\circ, L^\circ) = (t_{12}, \lambda_{12})$ is unsuitable for the study of the dust-molecule mixture.

5.4 The Vlasov-Boltzmann model when $t^\circ = t_{12}$ and $L^\circ = \lambda_{12}/\sqrt{\varepsilon}$

We considere the time and space scales defined by (111)(b) and (114)(b). In that case, system (107) is given by

$$\left\{ \begin{array}{l} \dfrac{\partial \hat{f}_1}{\partial \bar{t}} + \sqrt{\varepsilon}\, \hat{v}_1 \cdot \nabla_{\bar{x}} \hat{f}_1 + \dfrac{\sqrt{\varepsilon}}{\pi}\ \bar{\Upsilon}_a(\check{f}_2)(\bar{t}, \bar{x}, \hat{v}_1, \bar{r}) \cdot \nabla_{\hat{v}_1} \hat{f}_1 = 0, \quad \text{(a)} \\ \\ \dfrac{\partial \check{f}_2}{\partial \bar{t}} + \check{v}_2 \cdot \nabla_{\bar{x}} \check{f}_2 = \dfrac{\alpha^\circ}{\pi}\ \bar{R}_2(\hat{f}_1, \check{f}_2) + \dfrac{1}{\pi} \left(\dfrac{r_2}{r^\circ}\right)^2 \bar{Q}(\check{f}_2, \check{f}_2). \qquad \text{(b)} \end{array} \right. \tag{120}$$

Thanks to Hypothesis 2-4, we notice that system (120) is close to

$$\left\{\begin{array}{ll} \dfrac{\partial \hat{f}_1}{\partial \bar{t}} = 0, & \text{(a)} \\ \\ \dfrac{\partial \check{f}_2}{\partial \bar{t}} + \check{v}_2 \cdot \nabla_{\bar{x}} \check{f}_2 = 0. & \text{(b)} \end{array}\right. \tag{121}$$

Thus, the choice $(t^\circ, L^\circ) = (t_{12}, \lambda_{12}/\sqrt{\varepsilon})$ is also unsuitable for the study of the dust-molecule mixture.

5.5 The Vlasov-Boltzmann model when $t^\circ = t_{22}$ and $L^\circ = \sqrt{\varepsilon}\ \lambda_{22}$

We considere the time and space scales defined by (111)(a) and (115)(a). In that case, system (107) is given by

$$\left\{\begin{array}{ll} \dfrac{\partial \hat{f}_1}{\partial \bar{t}} + \hat{v}_1 \cdot \nabla_{\bar{x}} \hat{f}_1 + \dfrac{\sqrt{\varepsilon}}{4\pi\sqrt{2}} \left(\dfrac{r^\circ}{r_2}\right)^2 \bar{\Upsilon}_a(\check{f}_2)(\bar{t}, \bar{x}, \hat{v}_1, \bar{r}) \cdot \nabla_{\hat{v}_1} \hat{f}_1 = 0, & \text{(a)} \\ \\ \sqrt{\varepsilon} \dfrac{\partial \check{f}_2}{\partial \bar{t}} + \check{v}_2 \cdot \nabla_{\bar{x}} \check{f}_2 = \dfrac{\sqrt{\varepsilon}}{4\pi\sqrt{2}} \alpha^\circ \left(\dfrac{r^\circ}{r_2}\right)^2 \bar{R}_2(\hat{f}_1, \check{f}_2) + \dfrac{\sqrt{\varepsilon}}{4\pi\sqrt{2}} \bar{Q}(\check{f}_2, \check{f}_2). & \text{(b)} \end{array}\right. \tag{122}$$

Moreover, we have

$$\frac{\sqrt{\varepsilon}}{4\sqrt{2}} \left(\frac{r^\circ}{r_2}\right)^2 \simeq 1$$

under Hypothesis 10 (*cf.* (109)). Thus, we obtain that system (122) is close to

$$\left\{\begin{array}{ll} \dfrac{\partial \hat{f}_1}{\partial \bar{t}} + \hat{v}_1 \cdot \nabla_{\bar{x}} \hat{f}_1 + \dfrac{c_1}{\pi} \bar{\Upsilon}_a(\check{f}_2)(\bar{t}, \bar{x}, \hat{v}_1, \bar{r}) \cdot \nabla_{\hat{v}_1} \hat{f}_1 = 0, & \text{(a)} \\ \\ \sqrt{\varepsilon} \dfrac{\partial \check{f}_2}{\partial \bar{t}} + \check{v}_2 \cdot \nabla_{\bar{x}} \check{f}_2 = 0 & \text{(b)} \end{array}\right. \tag{123}$$

where c_1 is a constant of order one. Thus, the choice $(t^\circ, L^\circ) = (t_{22}, \sqrt{\varepsilon}\ \lambda_{22})$ is also unsuitable for the study of the dust-molecule mixture.

5.6 The Vlasov-Boltzmann model when $t^\circ = t_{22}$ and $L^\circ = \lambda_{22}$

We considere the time and space scales defined by (111)(a) and (115)(b). In that case, system (107) is given by

$$\left\{\begin{array}{ll} \dfrac{\partial \hat{f}_1}{\partial \bar{t}} + \sqrt{\varepsilon}\, \hat{v}_1 \cdot \nabla_{\bar{x}} \hat{f}_1 + \dfrac{\sqrt{\varepsilon}}{4\pi\sqrt{2}} \left(\dfrac{r^\circ}{r_2}\right)^2 \bar{\Upsilon}_a(\check{f}_2)(\bar{t}, \bar{x}, \hat{v}_1, \bar{r}) \cdot \nabla_{\hat{v}_1} \hat{f}_1 = 0, & \text{(a)} \\ \\ \dfrac{\partial \check{f}_2}{\partial \bar{t}} + \check{v}_2 \cdot \nabla_{\bar{x}} \check{f}_2 = \dfrac{1}{4\pi\sqrt{2}} \alpha^\circ \left(\dfrac{r^\circ}{r_2}\right)^2 \bar{R}_2(\hat{f}_1, \check{f}_2) + \dfrac{1}{4\pi\sqrt{2}} \bar{Q}(\check{f}_2, \check{f}_2). & \text{(b)} \end{array}\right. \tag{124}$$

Thus, by taking into account (108) and (109), we can rewrite (124) with

$$\left\{\begin{array}{ll} \dfrac{\partial \hat{f}_1}{\partial \bar{t}} + \sqrt{\varepsilon}\, \hat{v}_1 \cdot \nabla_{\bar{x}} \hat{f}_1 + \dfrac{c_1}{\pi} \bar{\Upsilon}_a(\check{f}_2)(\bar{t}, \bar{x}, \hat{v}_1, \bar{r}) \cdot \nabla_{\hat{v}_1} \hat{f}_1 = 0, & \text{(a)} \\ \\ \dfrac{\partial \check{f}_2}{\partial \bar{t}} + \check{v}_2 \cdot \nabla_{\bar{x}} \check{f}_2 = \dfrac{c_2}{\pi} \bar{R}_2(\hat{f}_1, \check{f}_2) + \dfrac{1}{4\pi\sqrt{2}} \bar{Q}(\check{f}_2, \check{f}_2) & \text{(b)} \end{array}\right. \tag{125}$$

where, under Hypothesis 9 and 10, c_1 and c_2 are two constants of order one (*cf.* (108) and (109)). Thus, the choice $(t^\circ, L^\circ) = (t_{22}, \lambda_{22})$ seems to be appropriate for the theoritical and numerical study of the dust-molecule mixture. Moreover, the factor $\sqrt{\varepsilon}$ in front of the term $\hat{v} \cdot \nabla_{\bar{x}} \hat{f}_1$, related to the spatial variation

of the transport of dust particles, suggests that the displacement of dust particles is weak compared to the displacement of gas molecules. At last, we refer to [12] for a theorical study of the convergence of the solution of the spatially homogeneous system (124) when $\varepsilon \to 0$ for a fixed ratio $\frac{\sqrt{\varepsilon}}{4\pi\sqrt{2}}\left(\frac{r^\circ}{r_2}\right)^2$, but with operators $R_1(f_1,f_2)$ and $R_2(f_1,f_2)$ for which collisions between dust particles and gas molecules are described by (40) (and, thus, are elastic) rather than by Hypothesis 7.

Remark 1 *The constant c_2 can be linked to λ_{22} and λ_{21} defined by (26)(b) and (26)(d) respectively and under Hypothesis 8 :*

$$c_2 = \frac{\lambda_{22}}{\lambda_{21}}. \tag{126}$$

Thus, we recover the fact that $C_2 = O(1)$ under hypothesis 8-9 by using (116)

6 Numerical results

We now present homogeneous and 3D inhomogeneous numerical simulations of Boltzmann-Boltzmann system (37), of Vlasov-Boltzmann system (105) and of the more accurate Vlasov-Boltzmann system (106). These numerical results validate and justify (from a computational cost point of view) the derivation of asymptotic models (105) and (106). For the sake of simplicity, we considere in this section the situation of dust particles with an unique radius:

Hypothesis 11 *All particules have the same radius r_1.*

We still denote ε the ratio of mass $\varepsilon(r_1)$ given by (5)(b).

Let us note that in order to assess the efficiency of the numerical models from a computational cost point of view, or in order to simplify the visualization of the numerical results, we do not always use exactly the orders of magnitude of n_1°, n_2° and r_{min} given by (17) (more precisely, there is sometimes a factor 10 between the order of magnitudes used in section 2 and those used in this section). Nevertheless, Hypothesis 2-4 are always satisfied.

6.1 The Boltzmann-Boltzmann model

We now describe the numerical method used to discretize Boltzmann-Boltzmann system (37), and we propose a 3D numerical simulation of a LOVA scenario in a cubic box. Then, we underline the limitation of Boltzmann-Bolzmann system (37) because of the computational cost of simulations.

Under Hypothesis 11, we can remove the dependency in r of f_1. Then, weak formulations (57) and (59) of respective operators $R_1(f_1,f_2)$ and $R_2(f_1,f_2)$ are now given by

$$\begin{aligned}\int_{\mathbb{R}^3} \varphi(v) R_1(f_1,f_2)(t,x,v)dv = \int_{\mathbb{S}^2}\int_{\mathbb{R}^3}\int_{\mathbb{R}^3}\int_{\mathbb{R}^3} & \left[\varphi(v_1')-\varphi(v_1)\right] f_1(t,x,v_1) f_2(t,x,v_2) \\ & \times \varsigma(v_1-v_2,n) h_n(w) dn dw dv_1 dv_2\end{aligned} \tag{127}$$

and

$$\begin{aligned}\int_{\mathbb{R}^3} \varphi(v) R_2(f_1,f_2)(t,x,v)dv = \int_{\mathbb{S}^2}\int_{\mathbb{R}^3}\int_{\mathbb{R}^3}\int_{\mathbb{R}^3} & \left[\varphi(v_2')-\varphi(v_2)\right] f_1(t,x,v_1) f_2(t,x,v_2) \\ & \times \varsigma(v_1-v_2,n) h_n(w) dn dw dv_1 dv_2\end{aligned} \tag{128}$$

where

$$\varsigma(v,n) = (r_1+r_2)^2 \left[n\cdot v\right] 1_{\{n\cdot v\geq 0\}}. \tag{129}$$

Several numerical methods are used for the simulation of the Boltzmann equation (we refer to [38] for a review of these methods). One of these methods is the probabilistic Monte-Carlo method [39] whose advantage is the lower cost of computation compared to the cost of computation of a deterministic method. In the sequel, we adapt a classical Monte-Carlo method – namely, the Direct Simulation Monte-Carlo method *i.e.* DSMC method which is also known as the Bird's method – for the simulation of Boltzmann-Boltzmann system (37).

6.1.1 Monte-Carlo method

The Monte-Carlo method that we will present is a particle method. Thus, this numerical method is based on the principle which consists in approaching the distribution $f_i(t,x,v)$ with

$$f_i(t,x,v) \simeq \sum_{k=1}^{N_i} \omega_i^k \delta(x - x_i^k(t))\delta(v - v_i^k(t)) \tag{130}$$

for $i \in \{1,2\}$. From an heuristic point of view, (130) means that distribution f_1 (respectively f_2) in dust particles (respectively gas molecules) is approached by a number N_1 (respectively N_2) of macro-dust (respectively macro-molecule) characterized by positions $(x_1^k)_{k\in\{1,\dots,N_1\}}$, velocities $(v_1^k)_{k\in\{1,\dots,N_1\}}$ and weight factors $(\omega_1^k)_{k\in\{1,\dots,N_1\}}$ (respectively $(x_2^k)_{k\in\{1,\dots,N_2\}}$, $(v_2^k)_{k\in\{1,\dots,N_2\}}$ and $(\omega_2^k)_{k\in\{1,\dots,N_2\}}$). We take the same weight factor ω_i ($i \in \{1,2\}$) for every macro-dust ($i=1$) and for every macro-molecule ($i=2$), that is to say $\omega_i^k = \omega_i$ for every $(i,k) \in \{1,2\} \times \{1 \dots N_i\}$. We solve (37) with a splitting technique adapted to a Boltzmann type equation [22, 23]. This technique consists, firstly, in solving the transport equation

$$\begin{cases} \dfrac{\partial f_1}{\partial t} + v \cdot \nabla_x f_1 = 0, & \text{(a)} \\ \\ \dfrac{\partial f_2}{\partial t} + v \cdot \nabla_x f_2 = 0, & \text{(b)} \end{cases} \tag{131}$$

secondly, in solving the spacially homogeneous equation

$$\frac{\partial f_2}{\partial t} = Q(f_1, f_2) \tag{132}$$

and, thirdly, in solving the spacially homogeneous equations

$$\begin{cases} \dfrac{\partial f_1}{\partial t} = R_1(f_1, f_2), & \text{(a)} \\ \\ \dfrac{\partial f_2}{\partial t} = R_2(f_1, f_2). & \text{(b)} \end{cases} \tag{133}$$

Equations (131) are solved like in deterministic particle methods, that is to say particles are transported along characteristic lines and positions x_i^k are modified. Equations (132) and (133) are solved locally in each spacial mesh since collision operators have an effect only on velocities of particles and not on their positions. In each mesh c of volume V_c, f_1 and f_2 are approched by

$$f_i(t,v) \simeq \frac{\omega_i}{V_c} \sum_{k=1}^{N_{ic}} \delta(v - v_i^k(t)) \tag{134}$$

where N_{1c} (respectively N_{2c}) is the number of macro-dust (respectively macro-molecule) in the mesh c. Moreover, we can define the local density of each specie in the mesh c of volum V_c by

$$n_{ic} = \frac{N_{ic}\,\omega_i}{V_c} \tag{135}$$

for $i \in \{1,2\}$. The resolution of equations (132) and (133) during a time step Δt consists in determining the new velocities $(v_1^k(t+\Delta t))_{k\in\{1,\cdots,N_1\}}$ and $(v_2^k(t+\Delta t))_{k\in\{1,\cdots,N_2\}}$. The numerical resolution of equation (132) is made with the Bird's method with no time-counter [5, 4] ((132) is a classical homogeneous Boltzmann equation). Nevertheless, we cannot use the Bird's method to solve equations (133) because $\alpha^\circ := n_1^\circ/n_2^\circ \ll 1$ (see Hypothesis 4). Indeed, if we considere a macro-dust of velocity v_1 and a macro-molecule of velocity v_2, the probability that the first one collides the second one during the time Δt is given by

$$p_{12}(v_1, v_2) = \frac{\omega_2}{V_c}\,\Delta t\,\pi(r_1 + r_2)^2 |v_1 - v_2|$$

whereas the probability that the second one collides the first one during the time Δt is given by

$$p_{21}(v_1, v_2) = \frac{\omega_1}{V_c} \Delta t \, \pi (r_1 + r_2)^2 |v_1 - v_2|.$$

Then, the use of the Bird's method – which is characterized by the fact that $p_{12}(v_1, v_2) = p_{21}(v_1, v_2)$ (the Bird's method is a symetrical method [34]) – imposes to take the same weight factor ω_1 and ω_2 which implies that

$$\frac{N_{1c}}{N_{2c}} = \frac{n_{1c}}{n_{2c}}$$

by using (135). As a consequence, the estimate $\alpha^\circ \ll 1$ implies that $N_{1c} \ll N_{2c}$ and then we can either choose a reasonable number N_{2c} of macro-molecules with respect to the CPU time which implies a low number of macro-dust N_{1c} and then a poor accuracy, or choose a reasonable number of macro-dust N_{1c} with respect to accuracy and end up to a large number of macro-molecules N_{2c} which implies a huge CPU time.

Thus, if we want to have $\mathcal{O}(N_{1c}) = \mathcal{O}(N_{2c})$, we have to use a non-symetrical method. Here, we adapt the Nanbu's method for which equations (133)(a) and (133)(b) are solved separatly.

The Nanbu's algorithm for the simulation of $R_1(f_1, f_2)$ consists in two steps:

- **First step: Selection of pairs of collision.** Instead of computing the probability of collision $p_{12}(v_1, v_2)$ for every $N_{1c}N_{2c}$ possible pairs composed of a macro-dust of velocity v_1 and of a macro-molecule of velocity v_2, we use the fictive particle method. It consists in selecting

$$N_{1c}N_{2c} \frac{\omega_2}{V_c} \Delta t \, \pi (r_1 + r_2)^2 \, |v^{rel}|_{max} \tag{136}$$

  pairs composed of a macro-dust and of a macro-molecule with a uniform law on $\{1, \ldots, N_{1c}\} \times \{1, \ldots, N_{2c}\}$. In (136), $|v^{rel}|_{max}$ is an upper bound of the modulus of the relative velocity between macro-dusts and macro-molecules. For each selected pair, we determine if the collision occurs with the probability

$$p^f(v_1, v_2) = \frac{|v_1 - v_2|}{|v^{rel}|_{max}}$$

  where v_1 and v_2 are respectively the velocity of the macro-dust and of the macro-molecule. We select for that a real $p \in [0, 1]$ with a uniform law ; if $p \leq p^f$ then the velocity v_1 of the macro-dust is modified but the velocity v_2 of the macro-molecule remains the same ; if $p > p^f$ the velocities v_1 and v_2 remain the same.

- **Second step: Determination of the post-collisional velocity.** The post-collisional velocity v_1' of macro-dust is determined following the diffuse reflexion mechanism described in section 3.1: see Hypothesis 7. More precisely, for each collision between a macro-dust of velocity v_1 and a macro-molecule of velocity v_2, firstly, we have to compute n randomly in the half sphere delimited by $n \cdot (v_1 - v_2) \geq 0$. Secondly, a vector w is selected with the law h_n given by (45). Finally, the post-collisional velocity v_1' is given by

$$v_1' = \frac{1}{1 + \varepsilon}(v_1 + \varepsilon v_2 - \varepsilon w). \tag{137}$$

  We refere to [11] for further details.

The algorithm for the simulation of the operator $R_2(f_1, f_2)$ is identical (we just have to permut the subscripts 1 and 2, and to replace ε with $1/\varepsilon$ in (137)). The rigourous justification of this Nanbu's method for the resolution of system (133) with operators (127) and (128) should be possible like in [40]; this could be the subject of a forthcoming work. Moreover, the validity of this method has been studied in [10] for function $\varsigma(v, n)$ in operators (127) and (128) given by $\varsigma(v, n) = C$ (where C is a positive constant) instead of (129), knowing that in this particular case, it is possible to establish explicit formulae for the evolution of macroscopic velocities.

6.1.2 A 3D simulation in a cubic box

We present in this subsection an example of simulation of system (37) in a cubic geometry in a situation of a LOVA during a time $\mathcal{T}$. Initially, dust particles are lying on a thin layer of width a in the bottom of the box with the uniform density n_1 and there are no gas molecules inside the box. Then, a flow of molecules enters into the box through a square hole following a maxwellian distribution with a density n_2, a temperature T° and a macroscopic velocity V_m in the normal direction of the hole. The boundary conditions are diffuse reflexion except on the hole (for which the boundary condition is an emissive condition) and on the upper side of the box (where the boundary condition is an absorption condition).

Remark 2 *This last boundary condition enables to model a larger vacuum vessel than the box itself but to focus on the specific part of it where occurs a breach in the wall.*

We refere to [42] for the management of the boundary conditions. Dust particles are tungsten and the gas is composed of nitrogen molecules. The width of the box is noted L and the one of the hole is noted l. Geometrical parameters are given by

$$\begin{cases} L &= 10^{-2} \text{ m}, \\ l &= 5 \cdot 10^{-4} \text{ m}, \\ a &= 5 \cdot 10^{-4} \text{ m}. \end{cases} \tag{138}$$

Remark 3 *These rather small dimensions compared to the real ITER dimensions or to some representative work-up have been willfully chosen as so in order to test the initial Boltzmann-Boltzmann model which is much more expensive than the approximate Vlasov-Boltzmann model.*

Physical parameters are given by

$$\begin{cases} r_1 &= 5 \cdot 10^{-8} \text{ m}, \\ r_2 &= 10^{-10} \text{ m}, \\ n_1 &= 10^{15} \text{ m}^{-3}, \\ n_2 &= 10^{21} \text{ m}^{-3}, \\ T^\circ &= 300 \text{ K}, \\ T_{surf} &= 300 \text{ K}, \\ V_m &= 300 \text{ m} \cdot \text{s}^{-1} \end{cases} \tag{139}$$

and computation parameters are given by

$$\begin{cases} \text{number of meshes} &= 8000, \\ \text{number of processors} &= 64, \\ \text{final time of simulation} &= 45 \cdot 10^{-3} \text{ s}. \end{cases} \tag{140}$$

The final time $\mathcal{T}$ of the simulation has been obtained after a CPU time of simulation of 24×3600 s. One can observe on figure 2 that macro-dusts (represented by green spheres) are moved by the air ingress (some of the macro-molecules are represented by red spheres).

6.1.3 Limitation of the Boltzmann-Boltzmann model

The time of computation of Boltzmann-Boltzmann system (37) depends mainly on the number of collisions computed for the simulation of collision operators $R_1(f_1, f_2)$, $R_2(f_1, f_2)$ and $Q(f_2, f_2)$ at each time step. The

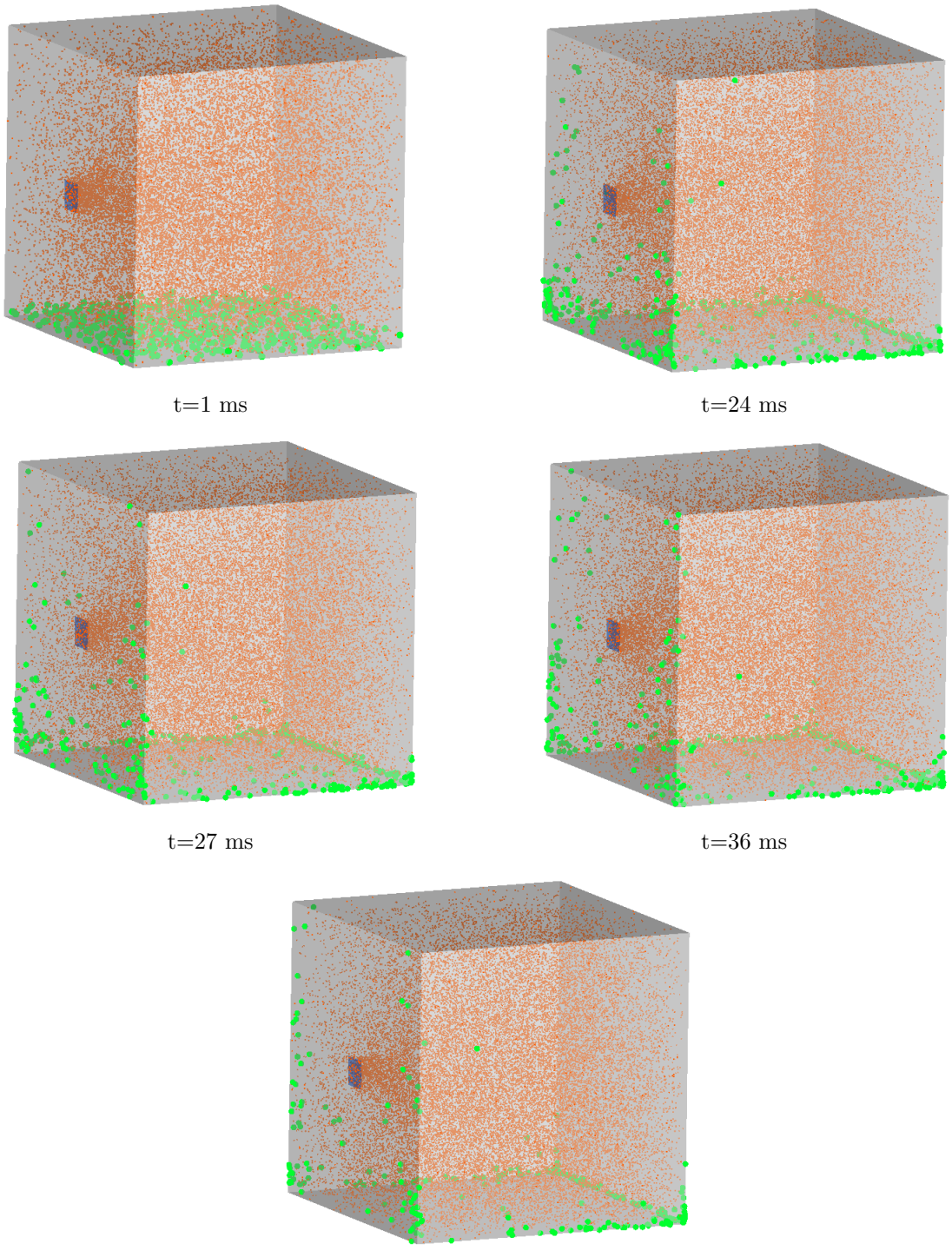

Figure 2: *LOVA type scenario in an open cubic box modeled with Boltzmann-Boltzmann system (37)*

average number of collisions computed for the simulation of $R_1(f_1, f_2)$, $R_2(f_1, f_2)$ and $Q(f_2, f_2)$ during a time τ in a mesh c is given by

$$\begin{cases} \overline{N_{R_1}}(\tau) = N_{1c} N_{2c} \dfrac{\omega_2}{V_c} \pi r_1^2 < V_{12}^{rel} > \tau, & \text{(a)} \\ \\ \overline{N_{R_2}}(\tau) = N_{1c} N_{2c} \dfrac{\omega_1}{V_c} \pi r_1^2 < V_{21}^{rel} > \tau, & \text{(b)} \\ \\ \overline{N_Q}(\tau) = \dfrac{1}{2} N_{2c}^2 \dfrac{\omega_2}{V_c} 4\pi r_2^2 < V_{22}^{rel} > \tau. & \text{(c)} \end{cases} \tag{141}$$

Since we have $\omega_i = n_{ic} V_c / N_{ic}$ (see (135)), $< V_2 > = < V_{22}^{rel} > / \sqrt{2}$ and $< V_2 > \simeq < V_{12}^{rel} > = < V_{21}^{rel} >$ (see section 5.1), we get

$$\frac{\overline{N_{R_1}}(\tau)}{\overline{N_{R_2}}(\tau)} = \frac{N_{1c}}{N_{2c}} \cdot \frac{n_{2c}}{n_{1c}}$$

and

$$\frac{\overline{N_{R_1}}(\tau)}{\overline{N_Q}(\tau)} \simeq \frac{1}{2\sqrt{2}} \cdot \frac{N_{1c}}{N_{2c}} \cdot \left(\frac{r_1}{r_2} \right)^2 .$$

If we choose N_{1c} and N_{2c} such that $N_{1c} \simeq N_{2c}$, thanks to Hypothesis 2 and 4, we obtain

$$\overline{N_{R_1}}(\tau) \gg \overline{N_{R_2}}(\tau)$$

and

$$\overline{N_{R_1}}(\tau) \gg \overline{N_Q}(\tau).$$

This brings into light that the simulation of the operator $R_1(f_1, f_2)$ is much costly than the other ones. Let us consider for example the simulation of equations (132) and (133) in an unique cell c with the following physical parameters

$$\begin{cases} r_1 &= 10^{-6}\,\mathrm{m}, \\ r_2 &= 2 \cdot 10^{-10}\,\mathrm{m}, \\ n_{1c} &= 10^{14}\,\mathrm{m}^{-3}, \\ n_{2c} &= 10^{21}\,\mathrm{m}^{-3}, \\ T^\circ &= 300\,\mathrm{K}. \end{cases} \tag{142}$$

Under these conditions and if we choose $N_{1c} \simeq N_{2c} \simeq 10^3$, the average numbers of collision during, for example, the time $\tau = 10^{-3}$ s are

$$\begin{cases} \overline{N_{R_1}}(\tau) \simeq 3 \cdot 10^{12}, \\ \\ \overline{N_{R_2}}(\tau) \simeq 3 \cdot 10^{5}, \\ \\ \overline{N_Q}(\tau) \simeq 4 \cdot 10^{5}. \end{cases}$$

We estimate that the time of computation of this example on a single-chip computer is of about $4,5 \cdot 10^6$ s that is to say 52 days. We conclude that the CPU time of the simulation of operator $R_1(f_1, f_2)$ could be extremely costly when the radius r_1 of dust particles becomes too large, even with massively parallel computation.

The limitation of Boltzmann-Boltzmann system (37) can also be seen from the point of view of the time step Δt. Indeed, it is possible to establish (see [11] for further details) that the Nanbu's method requires the condition on the time step

$$\Delta t \leq \min\left(t_{22}, t_{12}, t_{21}\right) \tag{143}$$

where t_{22}, t_{12} and t_{21} are defined by (111). Morever, the resolution of transport equations (131) requires the accuracy condition on the time step

$$\Delta t \lesssim \min\left(\frac{\Delta x}{< V_1 >}, \frac{\Delta x}{< V_2 >}\right) \tag{144}$$

where Δx is the length of meshes and where $< V_1 >$ and $< V_2 >$ are defined by (81). Finally, the condition on the time step is given by

$$\Delta t \leq \min\left(t_{22}, t_{12}, t_{21}, \frac{\Delta x}{< V_1 >}, \frac{\Delta x}{< V_2 >}\right). \tag{145}$$

Under physical conditions (142), we get

$$\begin{cases} t_{22} & \simeq & 2 \cdot 10^{-6} \text{ s}, \\ t_{12} & \simeq & 6 \cdot 10^{-13} \text{ s}, \\ t_{21} & \simeq & 6 \cdot 10^{-6} \text{ s}. \end{cases}$$

And, with the choice $\Delta x = 10^{-3}$ m which is, for physical parameters (142), the order of magnitude of the mean free path λ_{22} given by (26)(b) (since Hypothesis 9 is satisfied with the choice (142), λ_{22} is an appropriate characteristic length scale: see section 5.6), we get

$$\begin{cases} \dfrac{\Delta x}{< V_1 >} & \simeq & 30 \text{ s}, \\ \dfrac{\Delta x}{< V_2 >} & \simeq & 2 \cdot 10^{-5} \text{ s}. \end{cases}$$

Then, conditions (143) and (144) imply that

$$\Delta t \leq t_{12} \qquad \text{where} \qquad t_{12} \simeq 6 \cdot 10^{-13} \text{ s} \tag{146}$$

which is clearly too restrictive.

6.2 The Vlasov-Boltzmann model

We are now interested in the numerical method used to discretize the Vlasov-Boltzmann model (105) and the more accurate Vlasov-Boltzmann model (106) which, under Hypothesis 11, are respectively given by

$$\begin{cases} \dfrac{\partial f_1}{\partial t} + v \cdot \nabla_x f_1 + \Upsilon_a(f_2) \cdot \nabla_v (f_1) = 0, & \text{(a)} \\ \dfrac{\partial f_2}{\partial t} + v \cdot \nabla_x f_2 = R_2(f_1, f_2) + Q(f_2, f_2) & \text{(b)} \end{cases} \tag{147}$$

with

$$\Upsilon_a(f_2)(t,x) = \pi\, \varepsilon\, r_1^2 \int_{\mathbb{R}^3} f_2(t,x,v_2) \left[|v_2| + \frac{\sqrt{\pi}}{3\beta}\right] v_2 dv_2 \tag{148}$$

and by

$$\begin{cases} \dfrac{\partial f_1}{\partial t} + v \cdot \nabla_x f_1 + \nabla_v \cdot [\Upsilon_b(f_2) f_1] = 0, & \text{(a)} \\ \dfrac{\partial f_2}{\partial t} + v \cdot \nabla_x f_2 = R_2(f_1, f_2) + Q(f_2, f_2) & \text{(b)} \end{cases} \tag{149}$$

with

$$\Upsilon_b(f_2)(t,x,v_1) = \pi\, \varepsilon\, r_1^2 \int_{\mathbb{R}^3} f_2(t,x,v_2) \left[|v_2 - v_1| + \frac{\sqrt{\pi}}{3\beta}\right] (v_2 - v_1) dv_2 \tag{150}$$

(we recall that $\beta := \sqrt{\frac{m_2}{2k_B T_{surf}}}$, see (46), T_{surf} being the surface temperature of dust particles supposed to be constant for the sake of simplicity). We propose in section 6.2.2 spatially homogeneous simulations to validate Vlasov-Boltzmann models (147) and (149). And, we describe in section 6.2.3 a 3D numerical simulation obtained with Vlasov-Boltzmann system (149). This 3D simulation describes a LOVA type accident in a torus domain whose atmosphere is initially rarefied. We underline that this 3D test-case would be very expensive from a computational cost point of view if it was studied with the Boltzmann-Boltzmann system (37) instead of Vlasov-Boltzmann system (147) or (149).

6.2.1 PIC method coupled to Monte-Carlo method

Vlasov-Boltzmann system (147) (or (149)) is solved thanks to the coupling of a Particle-In-Cell (PIC) method for (147)(a) (or (149)(a)) and the Monte-Carlo method presented in section 6.1.1 for (147)(b) (or (149)(b)). Thus, the distribution in dust particles f_1 is still approached with

$$f_1(t,x,v) \simeq \omega_1 \sum_{k=1}^{N_1} \delta(x - x_1^k(t))\delta(v - v_1^k(t)).$$

Here, position x_1^k and velocity v_1^k of the macro-dusts are solutions of

$$\left\{ \begin{array}{ll} \dfrac{dx_1^k}{dt} = v_1^k, & \text{(a)} \\ \\ \dfrac{dv_1^k}{dt} = \Upsilon(f_2)(t, x_1^k, v_1^k) & \text{(b)} \end{array} \right. \tag{151}$$

where $\Upsilon(f_2)$ is given by (148) or (150). The term $m_1\Upsilon(f_2)$ models a drag force applied to a dust particle induced by collisions with gas molecules. This drag force – which is not deduced from experimental laws but from the asymptotic expansion proposed in section 4 – is also valid when the gas molecules are not at thermodynamical equilibrium. The term $\Upsilon(f_2)(t, x_1^k, v_1^k)$ is approched at each time t^n thanks to the local approximation of the density f_2 in each mesh c

$$f_2(t,x,v) \simeq \frac{\omega_2}{V_c} \sum_{j=1}^{N_{2c}} \delta(v - v_2^j(t)) 1_{\{x \in c\}}. \tag{152}$$

Then, system (151) is solved at each time step thanks to the following numerical scheme:

For all $k \in \{1, \ldots, N_{1c}\}$:

$$\left\{ \begin{array}{rcl} \dfrac{X_1^{k,n+1} - X_1^{k,n}}{\Delta t} & = & V_1^{k,n}, \\ \\ \dfrac{V_1^{k,n+1} - V_1^{k,n}}{\Delta t} & = & \Upsilon^{c,n}(V_1^{k,n}) \end{array} \right. \tag{153}$$

where $\Upsilon^{c,n}(V_1^{k,n})$ is a local approximation of $\Upsilon(f_2)(t^n, x_1^k, v_1^k)$ given by

$$\Upsilon_a^{c,n} = \pi\, \varepsilon\, r_1^2\, \frac{\omega_2}{V_c} \sum_{j=1}^{N_{2c}} \left[\left| V_2^{j,n} \right| + \frac{\sqrt{\pi}}{3\beta} \right] V_2^{j,n} \tag{154}$$

when $\Upsilon(f_2)$ is defined with (148), and by

$$\Upsilon_b^{c,n}(V_1^{k,n}) = \pi\, \varepsilon\, r_1^2\, \frac{\omega_2}{V_c} \sum_{j=1}^{N_{2c}} \left[\left| V_2^{j,n} - V_1^{k,n} \right| + \frac{\sqrt{\pi}}{3\beta} \right] \left(V_2^{j,n} - V_1^{k,n} \right) \tag{155}$$

when $\Upsilon(f_2)$ is defined with (150). Let us remark that in the case of $\Upsilon = \Upsilon_b$, the numerical resolution of (149)(a) requires the computation of the acceleration term $\Upsilon_b^{c,n}(V_1^{k,n})$ given by (155) for each macro-dust at

each time step, whereas in the case of $\Upsilon = \Upsilon_a$, the acceleration term $\Upsilon_a^{c,n}$ given by (154) is the same for all macro-dust in a given mesh c. Then, in each mesh c, the computational cost is in $\mathcal{O}(N_{2c})$ in the case of (154) and in $\mathcal{O}(N_{1c}N_{2c})$ in the case of (155).

The validity of this PIC method has been studied in [10] for the Vlasov-Boltzmann model obtained with the function $\varsigma(v,n) = C$ instead of (129) in operators (127) and (128).

Since we do not have to simulate the operator $R_1(f_1, f_2)$ any more, the condition on the time step is here given by

$$\Delta t \lesssim \min\left(t_{22}, t_{21}, \frac{\Delta x}{< V_1 >}, \frac{\Delta x}{< V_2 >}\right) \tag{156}$$

which is much more easier to achieve than condition (146). Let us note that under Hypothesis 8 and 9, we have $t_{22} \simeq t_{21}$ and $\lambda_{22} \simeq \lambda_{21}$ (see (113) and (116)), and we can choose $\Delta x = \mathcal{O}(\lambda_{22})$ (see section 5.6). As a consequence, we obtain $\mathcal{O}\left(\frac{\Delta x}{<V_1>}\right) = t_{22}/\sqrt{\varepsilon}$ and $\mathcal{O}\left(\frac{\Delta x}{<V_2>}\right) = t_{22}$ (by also using the fact that $\lambda_{ij} =< V_i > t_{ij}$ and that $< V_1 > / < V_2 > \simeq \sqrt{\varepsilon}$). Thus, in our context, (156) is equivalent to

$$\Delta t \lesssim t_{22}. \tag{157}$$

6.2.2 Comparison with the Boltzmann-Boltzmann model in an homogeneous context

We compare numerical simulations of Boltzmann-Boltzmann system (37) and of Vlasov-Boltzmann system (147) or (149) through the time evolution of macroscopic velocities and kinetic temperatures. We also compare Vlasov-Boltzmann systems obtained with $\Upsilon = \Upsilon_a$ (see (148)) and with $\Upsilon = \Upsilon_b$ (see (150)). At last, CPU times are compared. Let us note that these numerical simulations are obtained in an homogeneous context in order to get rid of the influence of boundary conditions.

Macroscopic velocities:

Figure 3 presents the evolution of macroscopic velocities defined by (16) obtained, firstly, with the numerical resolution of the spatially homogeneous system

$$\left\{\begin{array}{ll} \dfrac{\partial f_1}{\partial t} = R_1(f_1, f_2), & \text{(a)} \\ \\ \dfrac{\partial f_2}{\partial t} = R_2(f_1, f_2) + Q(f_2, f_2) & \text{(b)} \end{array}\right. \tag{158}$$

and, secondly, with the numerical resolution of the spatially homogeneous system

$$\left\{\begin{array}{ll} \dfrac{\partial f_1}{\partial t} + \nabla_v \cdot [\Upsilon(f_2) f_1] = 0, & \text{(a)} \\ \\ \dfrac{\partial f_2}{\partial t} = R_2(f_1, f_2) + Q(f_2, f_2) & \text{(b)} \end{array}\right. \tag{159}$$

where $\Upsilon(f_2) = \Upsilon_b(f_2)$ is given by (150), the initial distributions being given by

$$\left\{\begin{array}{rcl} f_{1,in}(v) & = & n_1 \left(\dfrac{2\pi k_B T_{1,in}}{m_1(r_1)}\right)^{-\frac{3}{2}} \exp\left(-\dfrac{m_1(r_1)\,|v - \mathbf{u}_{1,in}|^2}{2k_B T_{1,in}}\right), \\ \\ f_{2,in}(v) & = & n_2 \left(\dfrac{2\pi k_B T_{2,in}}{m_2}\right)^{-\frac{3}{2}} \exp\left(-\dfrac{m_2\,|v - \mathbf{u}_{2,in}|^2}{2k_B T_{2,in}}\right) \end{array}\right. \tag{160}$$

where

$$\begin{cases} \mathbf{u}_{1,in} &= (0,0,0)\ \mathrm{m}\cdot\mathrm{s}^{-1}, \\ \mathbf{u}_{2,in} &= (300,300,300)\ \mathrm{m}\cdot\mathrm{s}^{-1}, \\ T_{1,in} &= 100\,\mathrm{K}, \\ T_{2,in} &= 400\,\mathrm{K} \end{cases} \tag{161}$$

and

$$\begin{cases} r_1 &= 5\cdot 10^{-9}\ \mathrm{m}, \\ n_1 &= 10^{15}\ \mathrm{m}^{-3}, \\ n_2 &= 10^{20}\ \mathrm{m}^{-3}. \end{cases} \tag{162}$$

Moreover, we take $T_{surf} = 300$ K for the surface temperature of dust particles. Physical parameters (162) are chosen in order to allow to take a reasonable time step Δt for the resolution of system (158) with the numerical method presented in section 6.1.1: indeed, condition (143) gives $\Delta t \lesssim 2\cdot 10^{-7}$ s. Moreover, condition (157) gives $\Delta t \lesssim 2\cdot 10^{-5}$ s for the resolution of system (159) with the numerical method presented in section 6.2.1. Then, we chose respectively $\Delta t = 10^{-7}$ s for the resolution of system (158) and $\Delta t = 10^{-5}$ s for the resolution of system (159). Moreover, we chose $(N_1, N_2) = (5\cdot 10^2, 5\cdot 10^3)$ for the resolution of both systems (N_k is the number of macro-particles which approaches f_k through (134)).

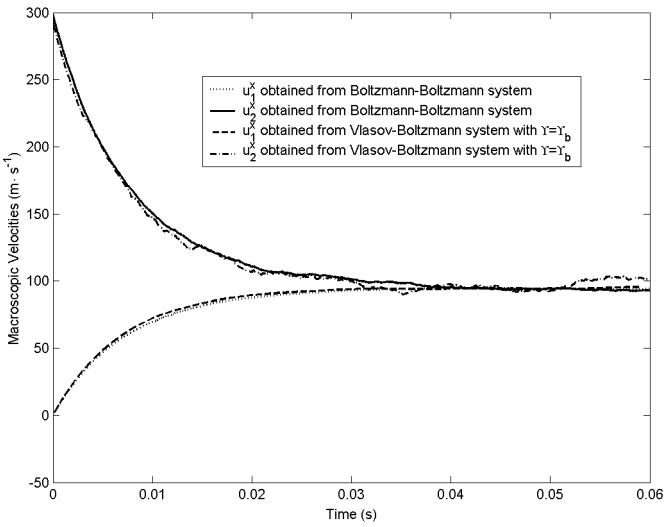

Figure 3: *Evolution of the component on Ox of macroscopic velocities obtained from the numerical resolution of systems* (158) *and* (159) *with* $\Upsilon = \Upsilon_b$

One can observe on figure 3 a similar evolution of components on Ox of macroscopic velocities – noted u_1^x and u_2^x – for the two systems. Moreover, it is quite obvious that these velocities converge to the value $94,5$ m·s^{-1} which corresponds to

$$u_\infty^x = \frac{n_1 u_{1,in}^x + \varepsilon n_2 u_{2,in}^x}{n_1 + \varepsilon n_2}.$$

This behaviour of macroscopic velocities corresponds to what could be expected for Boltzmann-Boltzmann system (37). Indeed, the following conservation of global momentum

$$n_1\mathbf{u}_1(t) + n_2\varepsilon\mathbf{u}_2(t) = n_1\mathbf{u}_{1,in} + n_2\varepsilon\mathbf{u}_{2,in}$$

can be obtained formally from equations (42) by using weak formulations (127) and (128) [11].

We now compare the evolution between macroscopic velocities obtained from the numerical resolution of system (159) with $\Upsilon = \Upsilon_a$ on one side and with $\Upsilon = \Upsilon_b$ on the other side, with initial conditions (160)(161) but with the physical parameters

$$\begin{cases} r_1 &= 5 \cdot 10^{-8} \text{ m}, \\ n_1 &= 10^{14} \text{ m}^{-3}, \\ n_2 &= 10^{21} \text{ m}^{-3} \end{cases}$$

instead of (162). We choose again $T_{surf} = 300$ K. Moreover, the numerical parameters are given by

$$\begin{cases} \Delta t &= 10^{-6} \text{ s}, \\ N_1 &= 5 \cdot 10^2, \\ N_2 &= 5 \cdot 10^3. \end{cases}$$

One can observe on figure 4 that the evolutions of these macroscopic velocities remain similar during a short

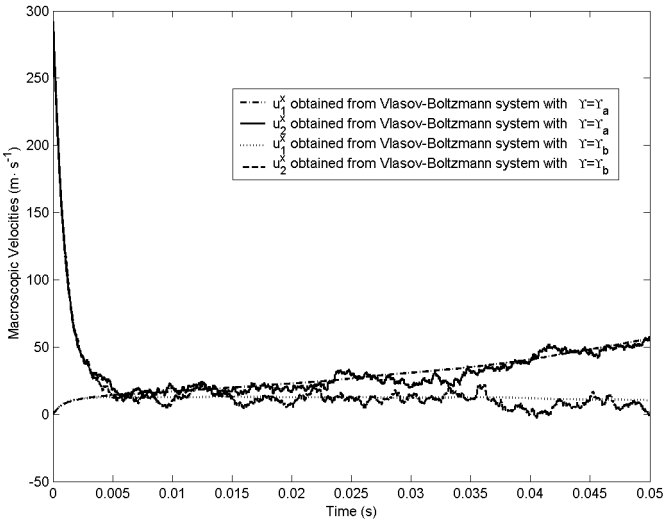

Figure 4: *Evolution of the component on Ox of macroscopic velocities obtained from the numerical resolution of system* (159) *with* $\Upsilon = \Upsilon_b$ *and with* $\Upsilon = \Upsilon_a$

time of about 5 ms but are different for long times. This can be interpreted in the following way: Whereas the global momentum $n_1\mathbf{u}_1 + n_2\varepsilon\mathbf{u}_2$ is conserved for Boltzmann-Boltzmann system (37) and approximately conserved for Vlasov-Boltzmann system (159) with $\Upsilon = \Upsilon_b$ given by (150), it is not the case for system (159) with $\Upsilon = \Upsilon_a$ given by (148). Since the expression of $\Upsilon_a(f_2)$ is obtained according to the hypothesis that the velocities of dust particles are of the order of magnitude of V_1° and that the velocities of gas molecules are of the order of magnitude of V_2° with $V_1^\circ/V_2^\circ = \sqrt{\varepsilon}$ (see (81) and (82)), we can consequently deduce that this velocity scaling hypothesis is only true during a short time (more precisely during a time of some ms in the present case).

Kinetic temperatures:

We present the comparison between the kinetic temperatures defined by (15) obtained from the numerical resolution of systems (158) and (159) (with $\Upsilon = \Upsilon_b$) with inital conditions (160)(161)(162). We choose again

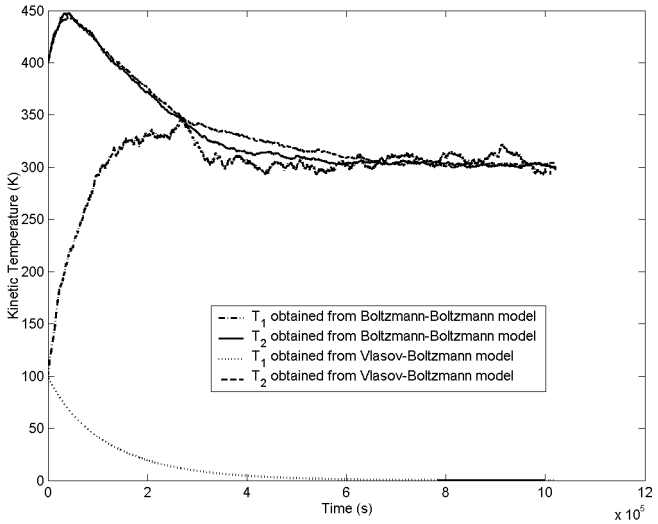

Figure 5: *Evolution of the kinetic temperatures obtained from numerical resolution of systems* (158) *and* (159) *with* $\Upsilon = \Upsilon_b$

$T_{surf} = 300$ K. One can observe on figure 5 that the kinetic temperatures T_{f_1} and T_{f_2} obtained from the numerical resolution of Boltzmann-Boltzmann system (158) converge to the surface temperature T_{surf} of dust particles. Moreover, the kinetic temperature T_{f_2} obtained from the numerical resolution of Vlasov-Boltzmann system (159) with $\Upsilon = \Upsilon_b$ has the same behaviour as the one of the kinetic temperature T_{f_2} obtained from the numerical resolution of Boltzmann-Boltzmann system (158). However, one can observe that T_{f_1} obtained from the numerical resolution of Vlasov-Boltzmann system (159) with $\Upsilon = \Upsilon_b$ converges to 0 and, thus, is wrong (we can make the same observation with $\Upsilon = \Upsilon_a$). We discuss this important point in section 6.2.5.

CPU times:

We now consider the initial distributions $f_{1,in}$ and $f_{2,in}$ given by (160)(161) but with the physical parameters

$$\left\{ \begin{array}{rcl} r_1 & = & 2 \cdot 10^{-8} \text{ m}, \\ n_1 & = & 5 \cdot 10^{13} \text{ m}^{-3}, \\ n_2 & = & 10^{20} \text{ m}^{-3} \end{array} \right. \tag{163}$$

instead of (162). We choose again $T_{surf} = 300$ K and we take $(N_1, N_2) = (10^2, 10^4)$. Because of conditions (143) and (157), the time step Δt is taken equal to $\Delta t = 10^{-8}$ s in the case of Boltzmann-Boltzmann system (158) and equal to $\Delta t = 2 \cdot 10^{-5}$ s in the case of Vlasov-Boltzmann system (159). During the time $\tau = 10^{-1}$ s (which corresponds to the characteristic time of relaxation of velocities), the average numbers (141) of collisions simulated for the resolution of the kinetic operators are of the order of

$$\left\{ \begin{array}{ll} \overline{N_{R_1}}(\tau) & = 1,4 \cdot 10^9, \\ \overline{N_{R_2}}(\tau) & = 7 \cdot 10^4, \\ \overline{N_Q}(\tau) & = 4,2 \cdot 10^7. \end{array} \right.$$

We see on Table 1 that the CPU time on a single-chip computer of the simulation of Boltzmann-Boltzmann system (158) during the time τ is of about 10^4 s, the one of system (159) with $\Upsilon = \Upsilon_b$ during the time τ is of about 500 s and the one of Vlasov-Boltzmann system (159) with $\Upsilon = \Upsilon_a$ during the time τ is of about 50 s.

Model	CPU time
Boltzmann-Boltzmann model (158)	11410
Vlasov-Boltzmann model (159) with $\Upsilon = \Upsilon_b$	589
Vlasov-Boltzmann model (159) with $\Upsilon = \Upsilon_a$	45

Table 1: *CPU time of simulations of systems* (158) *and* (159) *with parameters* (163)

6.2.3 A 3D simulation in a cubic box

We present on figure 6 the LOVA type scenario already studied in section 6.1.2 with Boltzmann-Boltzmann system (37) (see figure 2) but, now, obtained with Vlasov-Boltzmann system (149) ($\Upsilon = \Upsilon_b$ is given by (150)). The final time of the simulation is equal to 247 ms. On figure 6, the macro-molecules are not represented and the number of macro-dusts represented is more important than on figure 2. Let us underline that we are able to simulate this LOVA type scenario with a final time greater than the one of 45 ms simulated in section 6.1.2 with Boltzmann-Boltzmann system (37) because Vlasov-Boltzmann system (149) needs far less CPU time.

6.2.4 A 3D simulation in a torus domain

We present on figure 7 a LOVA type scenario for which the domain is a cylindrical torus whose geometry is similar to the one used in [43]. There is no absorption condition on any side which means that dust particles and gas molecules (which are not represented in this visualization) cannot leave the domain. As a consequence, the density of gas molecules inside the torus increases very quickly. The cylindrical torus has the dimensions

$$\left\{\begin{array}{lcl} \text{height} & = & 10^{-1} \text{ m}, \\ \text{interior radius} & = & 2,5 \cdot 10^{-2} \text{ m}, \\ \text{outer radius} & = & 5 \cdot 10^{-2} \text{ m}, \\ \text{volume} & = & 5,89 \cdot 10^{-4} \text{ m}^3. \end{array}\right. \tag{164}$$

Numerical parameters are given by

$$\left\{\begin{array}{lcl} \text{number of meshes} & = & 14400, \\ \text{number of processors} & = & 480, \\ \text{length of simulation} & = & 1,1 \text{ ms} \end{array}\right. \tag{165}$$

and physical parameters are given by (139). Because of the dimensions of the cylinder and the increasing density in gas molecules, the cost of computation is higher in this example, and the length of simulation is lower than in the example of paragraph 6.2.3 for the same CPU time (24×3600 s).

6.2.5 Justification of the Vlasov-Boltzmann model

The previous studies lead to the following conclusions:

- The CPU cost of the numerical resolution of Vlasov-Boltzmann system (147) or (149) is, in the context we consider, lower than the one of Boltzmann-Boltzmann system (37). For example, on a spatially

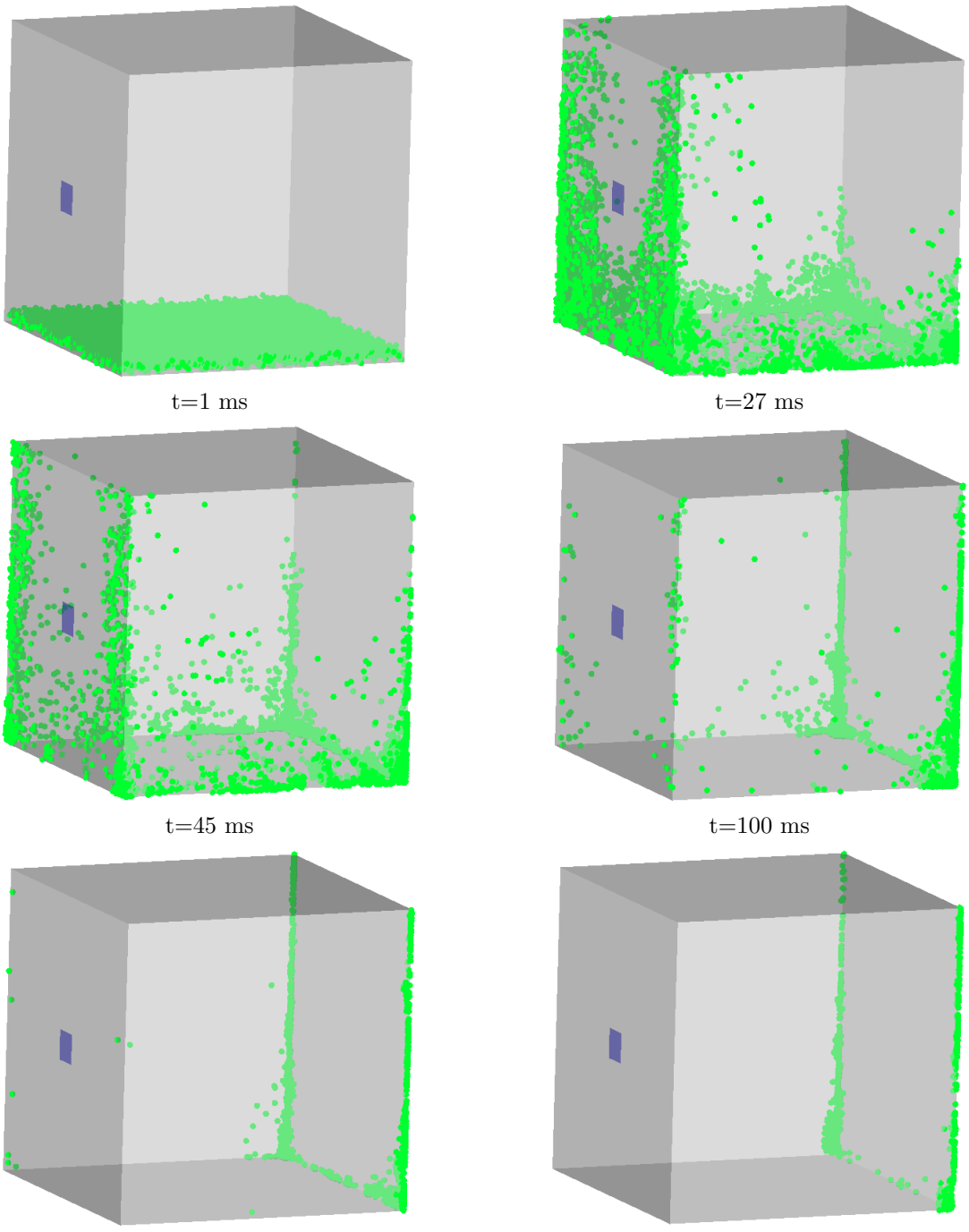

Figure 6: *LOVA type scenario in an open cubic box modeled with Vlasov-Boltzmann system (149)* ($\Upsilon = \Upsilon_b$)

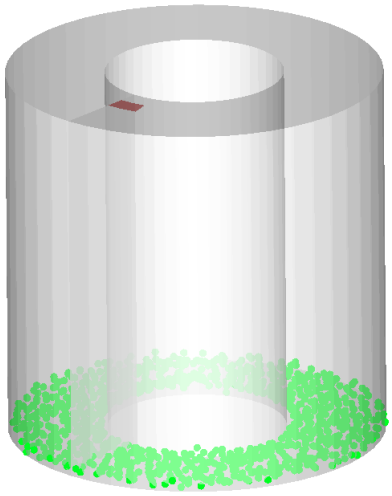

t= 0 ms

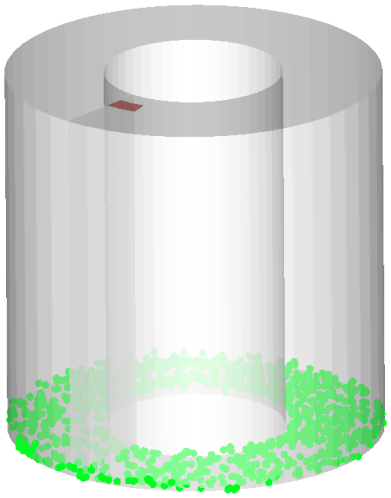

t= 0, 2 ms

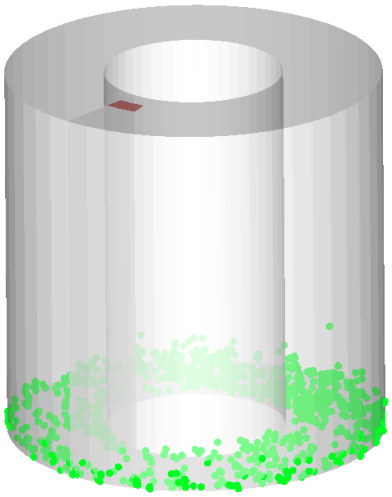

t= 0, 4 ms

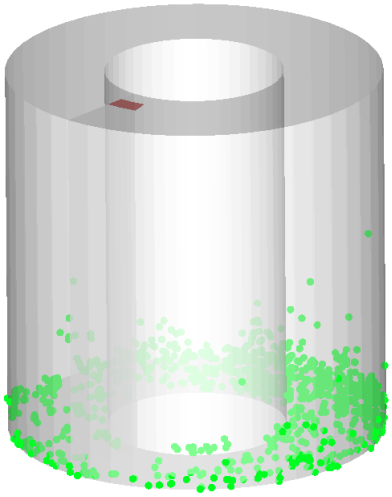

t= 0, 6 ms

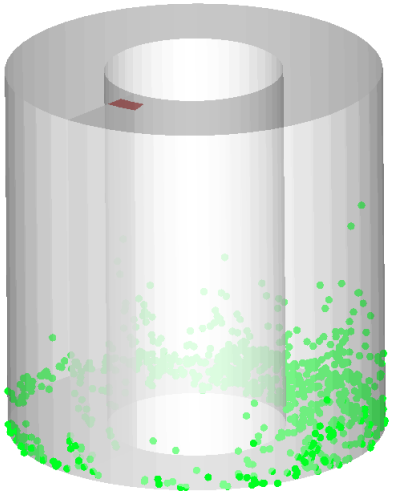

t= 0, 8 ms

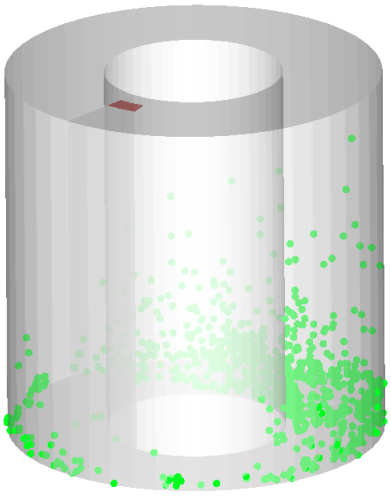

t= 1, 1 ms

Figure 7: *LOVA type scenario in a torus modeled with Vlasov-Boltzmann system (149)* ($\Upsilon = \Upsilon_b$)

homogeneous context, the examples presented on Table 1 show that the numerical resolution of Vlasov-Boltzmann system with $\Upsilon = \Upsilon_a$ and $\Upsilon = \Upsilon_b$ are respectively about 200 and 20 time less costly (with the numerical methods presented in sections 6.1.1 and 6.2.1). This comes from the fact that the resolution of the Vlasov equations (105)(a) or (106)(a) is in this situation lower than the resolution of the equation (37)(a). Moreover, the cost of the resolution of systems (105) and (106) does not depend very much of the radius of particles, whereas the cost the resolution of equation (37)(a) increases quadratically with the radius of particles.

- The numerical resolution of Vlasov-Boltzmann system (147) is about 10 time less costly than the one of Vlasov-Boltzmann system (149) (at least for the homogeneous test-case studied in section 6.2.2: see Table 1).

- The macroscopic velocities $\mathbf{u}_1$ and $\mathbf{u}_2$ obtained with spatially homogeneous Vlasov-Boltzmann system (159) with $\Upsilon = \Upsilon_b$ given by (150) are close to those obtained with spatially homogeneous Boltzmann-Boltzmann system (158) and, thus, are correct. Nevertheless, these macroscopic velocities obtained with spatially homogeneous Vlasov-Boltzmann system (159) with $\Upsilon = \Upsilon_a$ given by (148) instead of $\Upsilon = \Upsilon_b$ are correct only for short times. Moreover, the kinetic temperature T_{f_1} obtained with spatially homogeneous Vlasov-Boltzmann system (159) with $\Upsilon = \Upsilon_a$ or $\Upsilon = \Upsilon_b$ is not equal to the one obtained with spatially homogeneous Boltzmann-Boltzmann system (158) and, thus, is not correct. This may be explained by the fact that the asymptotic expansion made in the section 4 is only at the first order in ε. Thus, we may think that Vlasov-Boltzmann system (147) ($\Upsilon = \Upsilon_a$) or (149) ($\Upsilon = \Upsilon_b$) is not a good approximation of Boltzmann-Boltzmann system (37), and that a asymptotic expansion of $R_1(f_1, f_2)$ at the second order in ε could be necessary. Nevertheless, since we are only interested in the mobilization of dust particles at the beginning of a LOVA type scenario and since this mobilization is a direct function of the macroscopic velocity $\mathbf{u}_1$ of dust particles, it is legitimate to think that Vlasov-Boltzmann system (149) ($\Upsilon = \Upsilon_b$) and even Vlasov-Boltzmann system (149) ($\Upsilon = \Upsilon_a$) are enough accurate (at least for a first study) to evaluate if dust particles are or are not mobilized for a given LOVA type scenario.

All these remarks justify the derivation of the Vlasov-Boltzmann system to model the beginning of a LOVA type scenario.

7 Conclusion

A discussion about characteristic time and length scales shows that the interaction between dust particles and gas molecules at the beginning of a Loss Of Vacuum Accident (LOVA) in the thermonuclear reactor ITER has to be modeled with a kinetic model. Thus, we have proposed a new Boltzmann type model to describe the evolution of macroscopic particles, as dust particles, in a rarefied atmosphere. This Boltzmann type model consists in a coupling of a Boltzmann type operator $R_1(f_1, f_2)$ – which describes the dust-molecule collisions from the point of view of dust particles – with another Boltzmann type operator $R_2(f_1, f_2)$ – which describes the dust-molecule collisions from the point of view of gas molecules –. This Boltzmann-Boltzmann model takes into account the macroscopic character of dust particles compared to gas molecules through a diffuse reflexion mechanism on the surface of dust particles in the kinematic relations of dust-molecule collisions. As a consequence, the Boltzmann type operators $R_1(f_1, f_2)$ and $R_2(f_1, f_2)$ are not classical Boltzmann operators.

However, the numerical simulation with a Monte-Carlo method of the operator $R_1(f_1, f_2)$ is too expensive from a computational cost point of view in the context of a LOVA when the typical size of dust particles is too large. Thus, we have proposed to replace $R_1(f_1, f_2)$ with a Vlasov operator obtained from $R_1(f_1, f_2)$ through a formal asymptotic expansion according to the ratio of mass between a gas molecule and a dust particle. As a consequence, the Boltzmann-Boltzmann model is replaced by a Vlasov-Boltzmann model. Let us underline that the Vlasov operator allows to define a drag force model applied to dust particles and induced by collisions with gas molecules. This drag force model – which is not deduced from experimental laws – is also valid when the gas molecules are not at thermodynamical equilibrium.

Numerical methods are proposed for the resolution of the Boltzmann-Boltzmann and Vlasov-Boltzmann models, and are applied for 3D numerical simulations of LOVA type scenarii for which the domain is a cubic

box or a cylindrical torus: these 3D numerical simulations show the mobilization of dust particles induced by the gas molecules ingress. Moreover, spatially homogeneous numerical results are compared from the point of view of macroscopic velocities, kinetic temperatures and CPU time. These numerical studies validate and justify (from a computational cost point of view) the use of the Vlasov-Boltzmann model instead of the Boltzmann-Boltzmann model.

A validation of the Boltzmann-Boltzmann and Vlasov-Boltzmann models for a LOVA type scenario could be obtained from an experimental point of view thanks to experimental visualizations which should be lead. However, even if a fluid-fluid or a fluid-kinetic modelling like in [43] seems to be inadapted at the beginning of a LOVA, it should be necessary to use this type of modelling after some times (depending of the size of the vessel). Indeed, the density of the gas increases rapidly in a closed geometry. Then, the computational cost of the simulation of the Vlasov-Boltzmann model becomes too important because of the large amount of collisions between gas molecules. Thus, an interesting prospect could be to couple the Vlasov-Boltzmann model with its fluid limit by using an approach similar to those proposed, for example, in [20] or [15]. Moreover, another interesting prospect is to model the interaction between the dust particles and the wall of the vessel. We propose in [11] a model of mobilization of dust particles which takes into account a dust-wall interaction. This model could be investigated from a numerical point of view in a forthcoming work.

At last, we underline that the Boltzmann-Boltzmann and Vlasov-Boltzmann models proposed in this work could also be used to model, as in [45], the interaction between dust particles coming from an intensive volcanic plume and a rarefied atmosphere as in the case of volcanoes on Jupiter's moon Io. The Boltzmann-Boltzmann and Vlasov-Boltzmann models could be more accurate since, in [45], the macroscopic character of dust particles is not taken into account in the kinematic relations of the kinetic model and since the feedback of dust particles on the gas molecules is not taken into account.

Acknowledgements

Authors want to thank P. Roblin for his participation to the 3D numerical simulations, and L. Desvillettes for fruitful discussions.

References

[1] R. Alexandre and C. Villani. On the Landau Approximation in Plasma Physics, Annales de l'Institut Henri Poincaré/Analyse non linéaire, **21** (1), pp. 61–95, 2004.

[2] M.R. Baer and J.W. Nunziato. A two-phase mixture theory for the deflagration-to-detonation transition (ddt) in reactive materials. International Journal of Multiphase Flow, **12**, pp. 861–889, 1986.

[3] C.M. Benson, D.A. Levin, J. Zhong, S.F. Gimelshein and A. Montaser. Kinetic model for simulation of aerosol droplets in high-temperature environments. Journal of Thermophysics and Heat Transfer, **18**(1), pp. 122–134, 2004.

[4] G.A. Bird. Direct simulation and the Boltzmann equation. *Physics of Fluids*, **13**(11), p. 2676-2681, 1970.

[5] G.A Bird. Monte Carlo simulation of gas flows. *Annual Review of Fluid Mechanics*, **10**, pp. 11–31, 1978.

[6] G.A. Bird. Molecular Gas Dynamics and the Direct Simulation of Gas Flows. Oxford University Press, 1994.

[7] L. Boltzmann. Leçons sur la théorie des gaz. Gauthier-Villars, 1905.

[8] Z. Xu, J.R. Travis and W. Breitung Benchmarking validations for dust mobilization models of gasflow code. Technical report, Institut f
"ur Kern-und Energietechnik, 2008.

[9] Z. Xu, J.R. Travis, W. Breitung and T Jordan Verification of a dust transport model against theoretical solutions in multidimensional advection diffusion problems. Fusion Engineering and Design. Elsevier, 2010.

[10] F. Charles. Kinetic modelling and numerical simulations using particle methods for the transport of dust in a rarefied gas. In *Rarefied Gas Dynamics: Proceedings of the 26th International Symposium on Rarefied Gas Dynamics.* pp. 409–414, 2008.

[11] F. Charles. Modélisation mathématiques et étude numérique d'un aérosol dans un gaz raréfié. Application à la simulation du transport de particules de poussière en cas d'accident de pert de vide dans ITER. PhD Thesis, École Normale Supérieure de Cachan, 2009.

[12] F. Charles and L. Desvillettes. Small mass ratio limit of Boltzmann equations in the context of the study of evolution of dust particles in a rarefied atmosphere. Journal of Statistical Physics, **137**(3), pp. 539–567, 2009.

[13] C. Cercignani. The Boltzmann Equation and its Applications. Applied Mathematical Sciences, **67**, Springer-Verlag, New-York, 1987.

[14] J.F. Crifo, G.A. Loukianov, A.V. Rodionov and V.V. Zakharov. Direct Monte Carlo and multifluid modelling of the circumnuclear dust coma spherical grain dynamics revisited. *Icarus*, **176**, n° 1, pp. 192–219, 2005.

[15] P. Degond, G. Dimarco and L. Mieussens. A multiscale kinetic-fluid solver with dynamic localization of kinetic effects. J. of Comp. Phys., **229**(13), pp. 4907-4933, 2010.

[16] P. Degond and B. Lucquin. The asymptotics of collision operators for two species of particule of disparate masses. Math. Mod. and Meth. in App. Sc., **6**(3), pp. 405–410, 1996.

[17] P. Degond and B. Lucquin-Desreux. Transport coefficients of plasmas and disparate mass binary gases. *Transport Theory and Statistical Physics*, **26**(6), pp. 595–633, 1996.

[18] P. Degond and B. Lucquin-Desreux. Comportement hydrodynamique d'un mélange gazeux formé de deux espèces de particules de masses très différentes. C. R. Acad. Sci. Paris Série I Math., **322**(4), pp. 405–410, 1996.

[19] P. Degond and B. Lucquin-Desreux. The Fokker-Planck asymptotics of the Boltzmann collision operator in the Coulomb case. Math. Mod. and Meth. in App. Sc., **2**(2), pp. 167–182, 1992.

[20] S. Dellacherie. Coupling of the Wang Chang–Uhlenbeck equations with the multispecies Euler system. J. of Comp. Phys., **189**(1), pp. 239–276, 2003.

[21] L. Desvillettes. On asymptotics of the Boltzmann equation when the collisions become grazing. Transport Theory and Statistical Physics, **21**(3), pp. 259–276, 1992.

[22] L. Desvillettes. On the convergence of splitting algorithms for some kinetic equations. *Asympt. Anal*, **6**(4), pp. 315–333, 1993.

[23] L. Desvillettes and S. Mischler. About the splitting algorithm for Boltzmann and B.G.K. equations. Math. Mod. and Meth. in App. Sc., **6**(8), pp. 1079–1101, 1996.

[24] G. Dufour. *Modélisation multi-fluide eulérienne pour les écoulements diphasiques à inclusions dispersées.* PhD thesis, ENSAE, 2005.

[25] G. Dufour, M. Massot and P. Villedieu. Étude d'un modèle de fragmentation secondaire pour les brouillards de gouttelettes. C. R. Acad. Sci. Paris Série I Math., **336**(5), pp. 447–452, 2003.

[26] E. Ferrari and L. Pareschi. Modelling and numerical methods for the dynamics of impurities in a gas. *International Journal for Numerical Methods in Fluids*, **57**(6), pp. 693-713, 2008.

[27] S. Østmo, A. Frezzotti and T. Ytrehus. Kinetic theory study of steady evaporation from a spherical condensed phase containing inert solid particles. Physics of Fluids, **9**(1), pp. 211–225, 1997.

[28] J.R Garcia-Cascales, J. Mulas-Pérez and H. Paillère. Extension of some numerical schemes to the analysis of gas and particle mixtures. *International Journal for Numerical Methods in Fluids*, **56**, pp. 845–875, 2008.

[29] D. Gidaspow. Hydrodynamics of fluidization and heat transfer: supercomputer modelling. *Applied Mechanics Review*, **39**, pp. 1–23, 1983.

[30] H. Grad. Asymptotic theory of the Boltzmann equation. *Physics of Fluids*, **147**(6), 1963.

[31] C. Grisolia, F. Onofr, and K.F. Ren. Développement d'un diagnostic optique des poussières en suspension dans le tokamac iter. In *Congrès Francophone de Techniques Laser*, 2008.

[32] S. Rosanvallon, C. Grisolia, G. Counsell, S.H. Hong, F. Onofri, J. Worms, J. Winter, B.M. Annaratone, G. Maddaluno and P. Gasior. Dust control in tokamak environment. Fusion Engineering and Design, **83**(10-12), pp. 1701–1705, 2008.

[33] J. Hylkema. *Modélisation cinétique et simulation numérique d'un brouillard dense de gouttelettes. Application aux propulseurs à poudre.* PhD thesis, ENSAE-Université Toulouse-III, 1999.

[34] B. Lapeyre, E. Pardoux and R. Sentis. Méthodes de Monte-Carlo pour les équations de transport et de diffusion. Springer, 1998.

[35] J. Mathiaud. Étude de systèmes de type gaz-particules. PhD thesis, École Normale Supérieure de Cachan, 2006.

[36] P.J. ORourke and A.A. Amsden. The TAB method for numerical calculation of spray droplet breakup. SAE Technical Paper 872089, 1987.

[37] S. Paci, N. Forgione, F. Parozzi, M.T. Porfiri. Bases for dust mobilization modelling in the light of STARDUST experiments. Nuclear Engineering and Design, Elsevier, **235** (10-12), pp. 1129–1138, 2005.

[38] L. Pareschi and G. Russo. An introduction to the numerical analysis of the Boltzmann equation. *Lecture Notes at M&KT, Riv. Mat. Univ. Parma*, **4**, pp. 145–250, 2005.

[39] L. Pareschi and G. Russo. An introduction to Monte Carlo methods for the Boltzmann equation. In *ESAIM : Proceedings*, 1999.

[40] B. Perthame. Introduction to the theory of random particle methods for Boltzmann equation. Technical Report 2218, INRIA, 1994.

[41] F. Onofri and K.F. Ren and C. Grisolia. Development of an in situ ITER dust diagnostic based on extinction spectrometry: Dedicated light scattering models. Journal of Nuclear Materials, Elsevier, **390**, pp. 1093–1096, 2009.

[42] P. Roblin. Documentation de référence du code DSMC. Technical report, SFME-LSET-RT-08-005-A, CEA Saclay, 2009.

[43] K. Takase. Three-dimensional numerical simulations of dust mobilization and air ingress characteristics in a fusion reactor during a LOVA event. *Fusion Engineering and Design*, **54**(3-4), pp. 605–615, 2001.

[44] J. Zhang, D. B. Goldstein, P. L. Varghese, N. E. Gimelshein, S. F. Gimelshein and D. A. Levin. Simulation of gas dynamics and radiation in volcanic plumes on Io. Icarus, **163**(1), pp. 182-197, 2003.

[45] J. Zhang, D.B. Goldstein, P.L. Varghese, L. Trafton, C. Moore and K. Miki. Numerical modeling of ionian volcanic plumes with entrained particulates. Icarus, **172**(2), pp. 479-502, 2004.